HHS Public Access

Author manuscript

Cell Rep. Author manuscript; available in PMC 2023 June 28.

Published in final edited form as:

Cell Rep. 2023 May 30; 42(5): 112500. doi:10.1016/j.celrep.2023.112500.

Vitamin K-dependent carboxylation regulates Ca^{2+} flux and adaptation to metabolic stress in β cells

Julie Lacombe[1,7,*], **Kevin Guo**[1,2,7], **Jessica Bonneau**[1,3], **Denis Faubert**[4], **Florian Gioanni**[1], **Alexis Vivoli**[5], **Sarah M. Muir**[1], **Soraya Hezzaz**[1], **Vincent Poitout**[5,6], **Mathieu Ferron**[1,2,3,6,8,*]

[1]Molecular Physiology Research Unit, Institut de Recherches Cliniques de Montréal, Montréal, QC H2W 1R7, Canada

[2]Division of Experimental Medicine, McGill University, Montréal, QC H4A 3J1, Canada

[3]Programme de Biologie Moléculaire, Université de Montréal, Montréal, QC H3T 1J4, Canada

[4]Mass Spectrometry and Proteomics Platform, Institut de Recherches Cliniques de Montréal, Montréal, QC H2W 1R7, Canada

[5]Montreal Diabetes Research Center, Centre de Recherche du Centre Hospitalier de l'Université de Montréal (CRCHUM), Montréal, QC H2X 0A9, Canada

[6]Département de Médecine, Université de Montréal, Montréal, QC H3T 1J4, Canada

[7]These authors contributed equally

[8]Lead contact

SUMMARY

Vitamin K is a micronutrient necessary for γ-carboxylation of glutamic acids. This post-translational modification occurs in the endoplasmic reticulum (ER) and affects secreted proteins. Recent clinical studies implicate vitamin K in the pathophysiology of diabetes, but the underlying molecular mechanism remains unknown. Here, we show that mouse β cells lacking γ-carboxylation fail to adapt their insulin secretion in the context of age-related insulin resistance or diet-induced β cell stress. In human islets, γ-carboxylase expression positively correlates with improved insulin secretion in response to glucose. We identify endoplasmic reticulum Gla protein (ERGP) as a γ-carboxylated ER-resident Ca^{2+}-binding protein expressed in β cells. Mechanistically, γ-carboxylation of ERGP protects cells against Ca^{2+} overfilling by diminishing STIM1 and Orai1 interaction and restraining store-operated Ca^{2+} entry. These results reveal a

*Correspondence: julie.lacombe@ircm.qc.ca (J.L.), mathieu.ferron@ircm.qc.ca (M.F.).

AUTHOR CONTRIBUTIONS

J.L. and M.F. conceived the study, designed the experiments, and initiated the project. J.L., K.G., D.F. and M.F. collected and analyzed data. J.B., F.G., S.M.M., and S.H. collected data. A.V. and V.P. prepared islet cDNA from rats infused with glucose. M.F. and J.L. wrote the manuscript, and all authors commented and contributed to editing the final version. M.F. acts as the guarantor of this work and is responsible for data access.

SUPPLEMENTAL INFORMATION

Supplemental information can be found online at https://doi.org/10.1016/j.celrep.2023.112500.

DECLARATION OF INTERESTS

The authors declare no competing interests.

critical role of vitamin K-dependent carboxylation in regulation of Ca^{2+} flux in β cells and in their capacity to adapt to metabolic stress.

Graphical Abstract

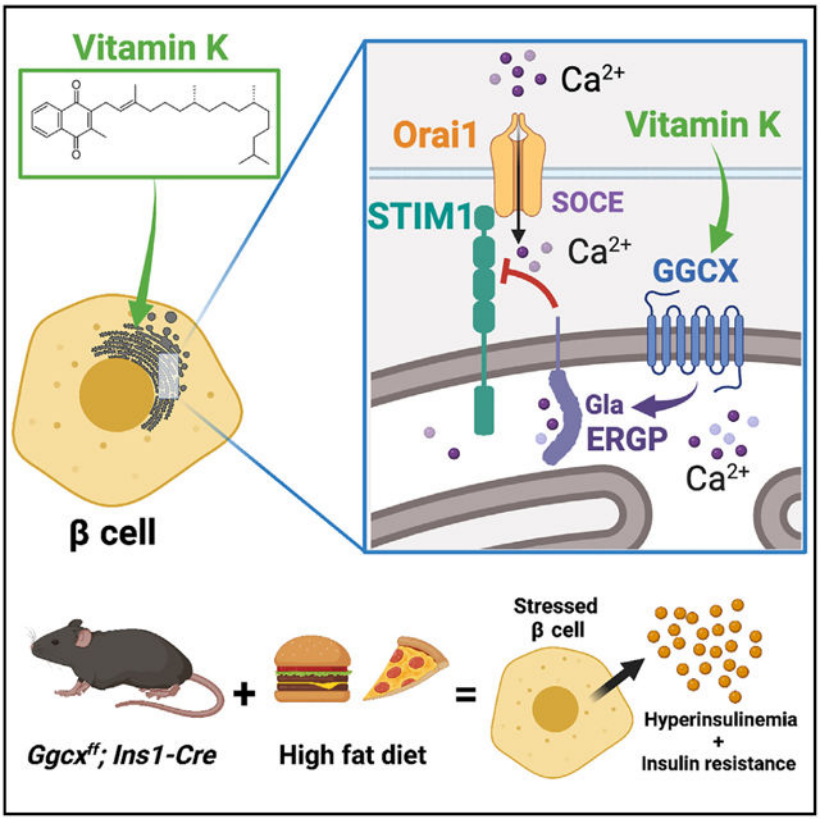

In brief

Reduced vitamin K (VK) intake is associated with an increased risk of developing type 2 diabetes. Lacombe et al. demonstrate that VK-dependent carboxylation is necessary for β cell adaptation in mice fed a high-fat diet. The underlying mechanism involves ERGP, a carboxylated protein that regulates store-operated calcium entry in β cells.

INTRODUCTION

Type 2 diabetes (T2D) is a metabolic disorder characterized by insulin resistance, hyperglycemia, and hyperinsulinemia.[1] Traditionally, T2D has been viewed as a disease initiated by peripheral insulin resistance, ultimately resulting in pancreatic β cell exhaustion. However, recent studies suggest that uncontrolled and excessive insulin secretion by β cells could be the driving force that elicits peripheral insulin resistance and metabolic complications in T2D.[2,3] Human and animal studies indicate that several factors can influence T2D susceptibility, including age, genetic variants, and diet. Many of these factors are thought to directly impact β cell function.[4] Increased consumption of highly processed, calorie-rich but nutrient-poor food is one possible contributor to the current

T2D pandemic.[5] Paradoxically, in Western countries, excess calorie intake is frequently associated with deficiencies in a number of micronutrients, including several vitamins.[6] Other studies have linked micronutrient deficiencies to an increased risk of diabetes.[7,8] Yet, the role of micronutrients in β cell function remains poorly understood.

Vitamin K (VK), a fat-soluble vitamin, functions as a co-factor during the γ-carboxylation reaction that converts glutamic acid (Glu) residues to γ-carboxyglutamic acid (Gla) residues in proteins transiting through the endoplasmic reticulum (ER). Two ER-resident enzymes are involved in this reaction, which together form the VK cycle: γ-glutamyl carboxylase (GGCX) and VK oxidoreductase (VKORC1).[9] GGCX requires reduced VK (VKH_2) as an essential cofactor, which, upon carboxylation of proteins, is oxidized to VK epoxide (VKO) and then reconverted to VKH_2 by VKORC1. The presence of this post-translational modification in proteins results in higher affinity for calcium ions (Ca^{2+}). Altogether, in vertebrates, less than 15 γ-carboxylated proteins have been identified so far, and all of them are secreted proteins. γ-Carboxylation is essential in the liver for the activity of several coagulation factors (e.g., prothrombin, factor IX, etc.) and in arteries and cartilage to modulate the activity of matrix Gla protein (MGP), which prevents extra-osseous tissue mineralization.[10,11] γ-Carboxylation also negatively regulates the function of osteocalcin, a bone-derived hormone with pleiotropic actions.[12,13] Whether γ-carboxylation occurs on ER-resident proteins and regulates cellular functions in a cell-autonomous manner is currently unknown.

Clinical and genetic data suggest that VK insufficiency or reduced VK intake are associated with an increased risk of developing metabolic syndrome or T2D.[14] Two longitudinal studies found a positive association between low dietary VK intake and risk of developing T2D.[15,16] It was also observed that 40% of morbidly obese patients are characterized by VK insufficiency and that low serum VK correlates positively with the presence of T2D in these subjects.[17–19] Finally, VK supplementation in patients with T2D significantly decreased their fasting glucose and HbA1c blood concentrations.[20,21] These clinical studies suggest a link between VK insufficiency and the risk of developing diabetes. However, they also raise important questions regarding the mechanism by which VK protects against T2D. Does VK directly affect β cell function? If so, what are the cellular and molecular mechanisms involved, and which γ-carboxylated protein mediates the protective effect of VK?

In the current study, we aimed to answer these questions using a combination of unique genetic, cellular, and biochemical tools we developed to study γ-carboxylation. Using loss-of-function models, we found that inactivation of *Ggcx* impairs β cell function in young mice exposed to a short bout of high-fat diet (HFD) feeding and compromises β cell survival in older animals fed a regular diet. Additionally, we identified ER Gla protein (ERGP) as a γ-carboxylated ER-resident protein that prevents Ca^{2+} overfilling by regulating store-operated Ca^{2+} entry (SOCE) in β cells. These data demonstrate that γ-carboxylation plays a critical role in the capacity of β cells to adapt to physiological stress and extend the cellular functions of this post-translational modification.

RESULTS

VK-dependent carboxylation occurs in islets and β cells

To identify tissue(s) involved in the beneficial effect of VK on glucose metabolism and T2D, we examined GGCX and VKORC1 protein levels in a panel of human tissues using the ProteomicsDB resource.[22] This analysis revealed that pancreatic islets were ranked fourth and first for GGCX and VKORC1 protein expression, respectively (Figure 1A), in agreement with our own data showing that *Ggcx* and *Vkorc1* genes are highly expressed in mouse islets (Figures S1A and S1B). To dissect *Ggcx* and *Vkorc1* expression within mouse islets, we used fluorescence-activated cell sorting to isolate β cells based on expression of the fluorescent reporter protein tdTomato (Tom) conditionally expressed in the insulin-positive cells of $Ins1^{Cre/+}$; $Rosa26^{CAG\text{-}lox\text{-}stop\text{-}lox\text{-}tdTomato}$ mice. Using this strategy, we obtained a pure β cell population (Tom^{+}), as demonstrated by expression of the insulin genes *Ins1* and *Ins2* and absence of the other endocrine cell type markers *Gcg*, *Ppy*, and *Sst* (Figure 1B). Further quantitative PCR (qPCR) analyses revealed that *Ggcx* and *Vkorc1* were expressed in β cells and other islet endocrine cells (Figure 1C). Tabula Muris single-cell transcriptomics data[23] confirmed *Ggcx* and *Vkorc1* expression in the endocrine pancreas (Figures S1C and S1D). These results agree with another set of publicly available mouse islet transcriptomics data.[24] In addition, we found that GGCX and VKORC1 proteins are expressed at similar and higher levels, respectively, in purified β cells compared with whole islets (Figure 1D). Using γ-carboxylated GGCX (Gla-GGCX) as a readout of a functional VK cycle,[25,26] we demonstrated that carboxylation does take place in pancreatic islets and specifically in β cells (Figure 1D). GGCX expression was also detected in the rat insulinoma cell line INS-1 832/3, and its γ-carboxylation was induced following treatment with phylloquinone (VK_1), which is absent from cell culture media and fetal bovine serum[27] (Figure 1E). To determine the extent of γ-carboxylation *in vivo* in islets and β cells, we isolated islets from $Ggcx^{ff}$; *Pdx1-Cre* and $Ggcx^{ff}$; *Ins1-Cre* mice in which *Ggcx* has been inactivated specifically in the pancreas or in β cells, respectively (Figures 1F, S1E, and S1F). Western blot analyses with a previously characterized α-Gla-specific antibody[26] revealed the presence of carboxylated proteins in islets and β cells, as demonstrated by reduced α-Gla immunoreactivity in $Ggcx^{ff}$; *Pdx1-Cre* and $Ggcx^{ff}$; *Ins1-Cre* islets (Figure 1F). Finally, GGCX expression was also detected in human islets, and culturing them with VK_1 significantly increased protein γ-carboxylation. Conversely, warfarin, an inhibitor of VKORC1 activity,[28] reduced it (Figures 1G and 1H; Table S1). We also observed that, in the presence of warfarin, GGCX migrates faster on SDS-PAGE because of its incomplete γ-carboxylation, in agreement with previous studies.[25,26] Together, these data indicate that VKORC1, GGCX, and γ-carboxylated proteins are present in islets and β cells.

Loss of γ-carboxylation induces a diabetic signature in islets

As a first step to determine the role of VK-dependent carboxylation in islets and β cells, we analyzed the expression profile of $Ggcx^{ff}$; *Pdx1-Cre* islets by RNA sequencing (RNA-seq). In comparison with control $Ggcx^{ff}$ islets, 319 genes were differentially expressed in $Ggcx^{ff}$; *Pdx1-Cre* islets (adjusted $p \leq 0.05$; Table S2). This set of genes was divided into two groups based on whether their expression was increased (114 genes) or decreased (205 genes) following *Ggcx* inactivation in islets, and a series of bioinformatics analyses

was completed. Gene set enrichment analyses with Gene Ontology revealed that many biological processes implicated in response to ER stress were significantly enriched within the group of genes downregulated in *Ggcx^{ff}; Pdx1-Cre* islets (Figure S2A). Similarly, when we interrogated the Kyoto Encyclopedia of Genes and Genomes (KEGG) pathway database, we found that this group of genes was enriched for pathways such as “apoptosis” and “protein processing in ER” (Figure S2B). Using the UniProt annotated keywords database, we observed, in the group of genes that were upregulated in *Ggcx^{ff}; Pdx1-Cre* islets, a very strong enrichment for protein keywords related to the secretory pathway (Figure S2C). We therefore hypothesized that the capacity of islet cells to respond and adapt to ER stress might be dysregulated in the absence of γ-carboxylation, potentially leading to impaired β cell function. In support of this notion, we found that a network of genes previously implicated in the β cell response to ER stress[29,30] was downregulated in the absence of γ-carboxylation (Figure S2D).

We next determined to which extent the transcriptome of *Ggcx^{ff}; Pdx1-Cre* islets intersects with the gene expression profile of islets from pre-diabetic (adult C57BL/6 mice on an HFD for 8 weeks) or diabetic (8-week-old *Lepr$^{db/db}$* and 7-week-old *Ire1α ^{ff}; Ins2-Cre$^{ERT/+}$*) mouse models.[31–33] 75% of the up- and 45% of the downregulated genes in *Ggcx^{ff}; Pdx1-Cre* islets were similarly dysregulated in at least one of these models (Figure S2E). About one-third of these genes encode proteins found within the secretory pathway (Figure S2F). The overlap between the transcriptome of *Ggcx^{ff}; Pdx1-Cre* islets and each mouse model was statistically significant for all comparisons (Table S3). Overall, these data suggest that loss of function of *Ggcx* in pancreatic endocrine cells induces a diabetic gene signature in these cells, presumably by altering their capacity to respond to ER stress.

GGCX is necessary for maintenance of an adequate β cell mass in adult mice

To determine the role of VK-dependent carboxylation in islet function *in vivo*, we next analyzed the metabolic consequences of pancreas-specific inactivation of *Ggcx* (*Ggcx^{ff}; Pdx1-Cre* mice). The *Pdx1-Cre* driver was selected because it resulted in efficient deletion in pancreatic islets[34] without expressing the human growth hormone (hGH).[35,36] The *Ggcx* mRNA level was reduced by more than 90%, and GGCX protein was undetectable in the pancreatic islets of these mice (Figures S1E and 1F). In agreement with efficient inactivation of GGCX, protein γ-carboxylation was abrogated in *Ggcx^{ff}; Pdx1-Cre* islets (Figure 1F). These mice did not display any differences in energy expenditure parameters (energy expenditure, O_2 consumption, and CO_2 release), physical activity, food intake, pancreas weight, and body weight (Figures S3A–S3E). In addition, inactivation of *Ggcx* occurred only in the pancreas of *Ggcx^{ff}; Pdx1-Cre* mice and not in any other tissue tested (Figure S3F).

A glucose tolerance test (GTT) revealed that an absence of γ-carboxylation in islets does not affect glucose handling in 16-week-old mice (Figure 2A). However, at 24 weeks of age, *Ggcx^{ff}; Pdx1-Cre* mice showed significantly elevated fasting blood glucose and decreased glucose tolerance (Figure 2B). This defect was traced to reduced circulating insulin following injection of glucose compared with the control mice (Figure 2C). Insulin sensitivity, assessed by an insulin tolerance test (ITT), appeared to be unaffected (Figure

2D). Pancreas immunohistochemistry revealed that β cell area and mass were reduced in *Ggcx*^{ff}*; Pdx1-Cre* mice at 32 weeks but not at 12 weeks of age (Figure 2E). Accordingly, total insulin content was diminished in the pancreas of 24- to 28-week-old *Ggcx*^{ff}*; Pdx1-Cre* mice (Figure 2F). β Cell area and β cell mass were also significantly lower in mice lacking the two VKORCs, *Vkorc1* and *Vkorc1l1*, in the pancreas only (Figures S3G–S3J), confirming involvement of the VK cycle in the observed phenotype.

By western blot using antibodies against cleaved caspase-3 and phospho(Ser139)-histone H2A.X, we detected apoptosis and DNA damage in *Ggcx*^{ff}*; Pdx1-Cre* islets older than 32 weeks but not in *Ggcx*^{ff} controls (Figure 2G). β Cell-specific apoptosis was independently confirmed using TUNEL and insulin co-staining on pancreas sections (Figures 2H and 2I). Importantly, β cell apoptosis, β cell mass, and pancreas insulin content were all unaffected in *Pdx1-Cre* mice (Figures 2H and S3K–S3L).

Static *ex vivo* glucose-stimulated insulin secretion (GSIS) experiments revealed a significant reduction in the capacity of the *Ggcx*-deficient (*Ggcx*^{ff}*; Pdx1-Cre*) islets to secrete insulin in response to glucose (Figure 2J), suggesting that γ-carboxylation is not only necessary to maintain a proper β cell mass but is also required for adequate insulin secretion in response to glucose in β cells.

Pancreas or β cell-specific deletion of Ggcx compromises insulin secretion in response to an HFD

Because the phenotype of the *Ggcx*^{ff}*; Pdx1-Cre* mice appears to be age dependent, we hypothesized that GGCX activity would be predominantly required when β cells need to adapt to stress such as age-related insulin resistance. To test GGCX involvement in acute β cell stress response, 10-week-old *Ggcx*^{ff}*; Pdx1-Cre* mice, which had not yet developed metabolic and β cell mass phenotypes (Figures 2A and 2E), were fed an HFD (60% kcal from fat) or a matched control low-fat diet (10% kcal from fat) for 7 days. This approach has been shown previously to induce β cell ER stress, glucose intolerance, and hyperinsulinemia in wild-type mice without significantly affecting peripheral insulin sensitivity.[37,38] qPCR analysis of ER stress markers on isolated islets confirmed that this short bout of HFD feeding induces ER stress in control and *Ggcx*^{ff}*; Pdx1-Cre* islets (Figures S4A–S4F). Interestingly, *Ddit3*, *Ppp1r15a*, and *Hspa5* were significantly more elevated in *Ggcx*^{ff}*; Pdx1-Cre* islets following short-term HFD feeding, while *sXbp1* was lower, suggesting a dysregulated unfolded protein response (UPR) in the absence of γ-carboxylation. This 7-day HFD feeding was also enough to increase body weight in mice regardless of the presence of *Ggcx* in their islets (Figure S4G). However, mice deprived of *Ggcx* expression in islets were not able to maintain their fed blood glucose level following HFD feeding (Figure 3A). The insulinemic response to glucose in absolute value or expressed as a stimulation index (SI; blood insulin concentration at 15 min or 30 min over T0) was not affected in the absence of *Ggcx* in mice fed the control diet (Figures 3B and 3C). In contrast, following 7 days on the HFD, *Ggcx*^{ff}*; Pdx1-Cre* mice showed a strong suppression of the SI, which was significantly lower than the SI of *Pdx1-Cre* control mice (Figures 3D and 3E). Of note, this impaired SI was associated with elevated fasting insulin (Figure 3F), while fasting glucose was not reduced, and glucose tolerance was moderately impaired (Figure S4H).

To determine whether GGCX affects β cell function in a cell-autonomous manner, we next analyzed *Ggcx^{ff}; Ins1-Cre* mice. At 10 weeks of age, *Ggcx^{ff}; Ins1-Cre* mice maintained on a regular chow diet had normal glucose tolerance, fasting glucose, and fasting insulin (Figured S4I–S4K). When *Ggcx^{ff}; Ins1-Cre* mice were fed an HFD for 7 days, no difference in body weight was noted (Figure S4L), but their fed glucose level was significantly increased (Figure 3G) and their SI was reduced (Figures 3H and 3I) in comparison to *Ins1-Cre* control mice fed the same HFD. Remarkably, in the same animals, fasting glucose was significantly increased (Figure 3J), although fasting serum insulin was also increased (Figure 3H). Glucose tolerance assessed through intraperitoneal or oral glucose load was unaffected (Figures S4M and S4N), suggesting a compensatory increase in insulin-independent glucose disposal.[39] Fasting hyperglycemia associated with hyperinsulinemia suggests peripheral insulin resistance. Accordingly, the homeostatic model assessment for insulin resistance (HOMA-IR) was increased in *Ggcx^{ff}; Ins1-Cre* mice on the HFD (Figure 3K), and insulin sensitivity evaluated by ITT was reduced in the same animals (Figure 3L). Together, these observations indicate that the absence of γ-carboxylation directly impacts β cells' capacity to adapt their insulin secretion in the face of metabolic stress, resulting in increased fasting insulin, loss of GSIS, and reduced peripheral insulin sensitivity.

To relate these findings to humans, we analyzed *GGCX* and *VKORC1* gene expression in human islets from 15 non-diabetic and diabetic donors and observed that the level of these two enzymes vary widely between donors but nevertheless strongly correlate with one another (Figure 3M; Table S1). This observation suggests that, for certain individuals, the γ-carboxylation machinery in their β cells might be more active compared with others. Further analysis revealed that *GGCX* expression levels positively and significantly correlate with the capacity of islets to secrete insulin in response to glucose ($r = 0.7181$, $\beta = 0.0026$; Figure 3N). The levels of *VKORC1* also positively correlate with the same parameter, although it did not reach statistical significance ($r = 0.4677$, $p = 0.0787$; Figures 3O). These results imply that γ-carboxylation could also impact GSIS in human β cells.

VK attenuates apoptosis induced by ER Ca^{2+} depletion

To determine whether VK and γ-carboxylation can protect β cells from the acute effects of ER stress, INS-1 832/3 β cells were cultured for 24 h in medium containing 25 mM glucose in the presence or absence of thapsigargin, an inhibitor of the sarcoplasmic reticulum/ER Ca^{2+}-ATPase (SERCA) and a pharmacological inducer of ER stress.[38] Doses of thapsigargin (10–40 nM) inducing moderate to elevated cell death in INS-1 cell cultures were selected based on previously published data.[40] Induction of Grp78/BiP and phospho(Ser724)-IRE following thapsigargin treatment confirmed the presence of ER stress and UPR (Figures S5A and S5B). In addition, western blots showed that thapsigargin dose-dependently induced apoptosis and DNA damage in β cells, while pre-treatment with VK_1 reduced the deleterious effects of 10 and 20 nM thapsigargin (Figure 4A). Interestingly, in the presence of thapsigargin, the GGCX protein level was increased by more than 2-fold, and its γ-carboxylation was also increased when VK_1 was included in the medium (Figure 4B). These results suggest that γ-carboxylation is activated in response to ER stress to protect β cells from apoptosis.

Glucose regulates VK-dependent carboxylation in β cells

We next sought to determine whether glucose itself, a physiological inducer of ER stress and UPR in β cells,[38] could regulate the VK cycle and γ-carboxylation. *Ggcx* and *Vkorc1* expression was increased at the mRNA and protein levels in response to 15 mM glucose in wild-type C57BL/6J mouse islets (Figures 4C and 4D). GGCX expression and γ-carboxylation were also induced when the rat β cell line INS-1 832/3 was cultured in the presence of high glucose (25 mM) concentrations (Figure 4E). To confirm that glucose regulates the VK cycle *in vivo*, 2-month-old Wistar rats were infused with glucose for 3 days and had their islets isolated, and gene expression was analyzed by qPCR. Glycemia reached ~15 mM in glucose-infused rats (Figure 4F), and this was sufficient to significantly increase *Ggcx* and *Vkorc1* expression in their islets (Figure 4G) compared with rats infused with saline solution, which maintained their blood glucose at ~7 mM. Finally, GGCX expression and global γ-carboxylation were also increased in non-diabetic human islets cultured for 3 days in medium containing 15 mM glucose (Figures 4H–4I; Table S1). These data indicate that glucose positively regulates the level and activity of the VK cycle in rodent and human β cells.

ERGP is a VK-dependent carboxylated protein expressed in β cells

In our mouse islet RNA-seq dataset, the genes encoding known γ-carboxylated proteins were all expressed at very low levels (Figure S6A). Together with detection in islets of multiple γ-carboxylated proteins by western blot (Figure 1F), these observations suggest that β cells express unknown Gla proteins.

Immunoprecipitation of γ-carboxylated proteins from 5-day old wild-type (WT) mouse liver extracts using our pan-specific α-Gla antibody led to identification of aspartyl/asparaginyl b-hydroxylase (ASPH) as a putative intracellular Gla protein (Table S4). The *Asph* locus contains two promoters (P1 and P2), undergoes extensive alternative splicing, and encodes three previously characterized ER-resident proteins: ASPH, junctate, and junctin (Figure S6B).[41,42] ASPH is expressed in several tissues under the control of P1, while junctate and junctin expression is controlled from P2 and appears to be restricted to cardiac and skeletal muscle.[43] ASPH is a type II transmembrane protein of ~80 kDa containing three luminal domains: an EF-hand Ca^{2+}-binding domain, a negatively charged Glu-rich domain (GRD) containing 39 Glu residues, and an alpha-ketoglutarate-dependent hydroxylase domain (Figure S6B). Junctate and junctin are ER-resident proteins corresponding to shorter variants of ASPH. Junctate and junctin share a different N-terminal cytosolic domain compared with ASPH, and junctin is characterized by a basic luminal domain instead of the acidic GRD domain found in junctate and ASPH (Figure S6B). Islet RNA-seq data indicate that the overall *Asph* expression level in islets is comparable with *Ggcx* and higher than any of the other genes encoding known γ-carboxylated proteins (Figure S6A). Our data also show that P2 is inactive in mouse islets, confirming that junctate and junctin isoforms are not expressed in these cells (Figures S6B and S6C). However, we detected a high level of expression for the last unique exon of junctate in islets, indicating that a truncated version of ASPH might be expressed in these cells. This shorter isoform was amplified by PCR on mouse islet cDNA using a pair of oligonucleotides located, respectively, in the first exon of ASPH (downstream of P1) and in the last exon of junctate. Sequencing of

the PCR product identified this transcript as *Asph* variant 4. The protein encoded by this transcript is identical to the first 308 amino acids (a.a.) of ASPH but lacks the last 433 a.a., including the hydroxylase domain (Figure S6B). Because this ER-resident protein appears to be γ-carboxylated (Table S4 and see below), we decided to name it ER Gla Protein (ERGP). The mRNAs encoding ASPH and ERGP are expressed in pancreatic islets, with ERGP mRNA being at least three times more expressed than ASPH mRNA (Figure S6C). Publicly available islet transcriptomics data further indicate that the mRNA of ASPH and ERGP, but not of junctate and junctin, are expressed in β cells (Figure S6B).[24] Based on these observations, we decided to determine whether ASPH and ERGP are the γ-carboxylated proteins detected in islets and β cells.

ASPH and ERGP share a GRD that could be prone to γ-carboxylation. To detect these two proteins, we generated and affinity purified rabbit polyclonal antibodies against the GRD domain; hereafter called α-A/E-GRD (Figures S6D and S6E). Importantly, addition of VK_1 or warfarin did not change the immunoreactivity of α-A/E-GRD antibodies against full-length ASPH and ERGP (Figure S6E). Anti-Gla immunoprecipitation (IP) followed by α-A/E-GRD western blotting or α-A/E-GRD IP followed by α-Gla western blotting confirmed that ASPH and ERGP are γ-carboxylated in 1-week-old WT liver but not in the liver of *Vkorc1*$^{-/-}$mice lacking γ-carboxylation at this age (Figures S6F and S6G).[26] Using the same approach, we could show that ASPH and ERGP are expressed and γ-carboxylated in adult control mouse islets and that their γ-carboxylation was greatly reduced in islets isolated from *Vkorc1*$^{-/-}$;*APOE-Vkorc1l1* mice, which have lower VKORCs activity and γ-carboxylation in all tissues except the liver (Figures 5A and S6H).[26] These analyses showed that ERGP expression and γ-carboxylation were, respectively, 7- and 8-fold higher than ASPH in control islets (Figure 5B). The same IP analysis performed on *Ggcx*^{ff}*; Ins1-Cre* islets revealed that ERGP, but not ASPH, is strongly γ-carboxylated in β cells (Figure 5C). Immunofluorescence on WT mouse islets confirmed expression of ERGP in islet endocrine cells, including β cells (Figure 5D). Finally, α-Gla IP followed by liquid chromatography-tandem mass spectrometry (LC-MS/MS) analyses on INS-1 832/3 cells cultured in 25 mM glucose and treated or not treated with 20 nM thapsigargin indicated that rat ERGP is also carboxylated in a VK-dependent manner in stressed β cells (Table S5; Figure S6I). Together these results establish that ERGP, and to a lesser extent ASPH, are γ-carboxylated proteins expressed in mouse β cells.

ERGP is γ-carboxylated on several Glu residues located in its GRD

To identify the domain(s) and specific Glu residues subjected to γ-carboxylation in ASPH and ERGP, we first expressed full-length ASPH-33FLAG or mutants lacking specific domains in HEK293 cells, a cell line that supports VK-dependent carboxylation.[26] Full-length ASPH γ-carboxylation was detected in cells cultured in the presence of VK_1, but not in presence of warfarin or when the GRD was deleted (Figure S6J). Although the a.a. sequence of the GRD is poorly conserved across mammalian species, the enrichment of Glu residues has been retained throughout evolution (Figure S6K). Internal deletions within the GRD of ERGP indicated that most of the γ-carboxylation sites are in the region encompassing residues 255–310 and/or that the C-terminal domain contains a critical sequence for recognition by GGCX (Figures 5E and 5F). We next mutated Glu residues

throughout the GRD into aspartic acid residues, which cannot be γ-carboxylated by GGCX (Figure 5E). Using this series of mutant proteins, we found that γ-carboxylated residues are mainly located in the N- and C-terminal regions of the GRD (Figures 5G and S6L), which was confirmed by LC-MS/MS analysis (Figures 5H and 5I; Table S6). No Gla-containing peptides were identified by the LC-MS/MS approach when ERGP was purified from HEK293 cells treated with warfarin or from *E. coli*, which lack γ-carboxylation machinery (Figure 5H).

We next tested whether γ-carboxylation could modulate the Ca^{2+}-binding capacity of ERGP.[11] Carboxylated and uncarboxylated ERGP-33FLAG were expressed and purified from HEK293 cells (Figure 5J) and $^{45}Ca^{2+}$ overlay experiments revealed that γ-carboxylated ERGP binds significantly more Ca^{2+} than its uncarboxylated counterpart (Figures 5K and 5L), suggesting that the presence of Gla residues in the GRD increases ERGP capacity to bind Ca^{2+}.

Carboxylated ERGP regulates SOCE

The cellular function of ERGP is unknown and, to our knowledge, has never been investigated. One study in T cells suggested that junctate acts as a Ca^{2+}-sensing ER protein regulating formation of stromal interaction molecule 1 (STIM1) and Orai1 protein complexes to activate SOCE, a cellular response whereby extracellular Ca^{2+} enters the cytosol following ER Ca^{2+} depletion to replete cellular Ca^{2+}.[44,45] SOCE is a prominent Ca^{2+} influx mechanism by which several cell types maintain cytosolic and ER Ca^{2+} levels at rest.[46,47] SOCE has been implicated in regulation of insulin secretion by β cells,[48] with loss of STIM1 leading to reduced insulin secretion and increased ER stress.[49] These observations prompted us to investigate whether ERGP and γ-carboxylation could affect cellular Ca^{2+} flux and SOCE.

To eliminate potential confounding effects caused by the endogenous human *ASPH* locus, we used CRISPR-Cas-9 genome editing to knock out all *ASPH* encoded isoforms in HEK293 cells (*ASPH*$^{-/-}$HEK293) (Figures S7A and S7B). The SOCE machinery was recapitulated in these cells by expressing STIM1-Myc and Orai1-hemagglutinin (HA) in the presence or absence of ERGP-33FLAG with or without VK_1 (Figure S7C). Carboxylated GGCX was detected in VK_1-treated cells regardless of ERGP expression, confirming efficient γ-carboxylation in these cells. Ratiometric cytosolic Ca^{2+} measurement with the Fluo-4 and Fura Red Ca^{2+} indicators was next used to assess SOCE, which was triggered first by depleting ER Ca^{2+} with thapsigargin in Ca^{2+}-free buffer, followed by Ca^{2+} addback to the buffer (Figure 6A). Using these experimental settings, we observed that cells expressing γ-carboxylated ERGP are characterized by a reduction in their ER Ca^{2+} release and SOCE (Figures 6B–6D). In addition, there was a significant reduction in basal cytosolic Ca^{2+} level in the same cells (Figures 6B and 6E), suggesting that ERGP, only when γ-carboxylated, restrains cytosolic Ca^{2+} in cells.

The impact of ERGP and of its carboxylation on ER Ca^{2+} levels was next assessed directly using the D4ER ratiometric ER-targeted fluorescence resonance energy transfer (FRET)-based Ca^{2+} sensor.[50] These analyses confirmed that, in the presence of γ-carboxylated ERGP, HEK293 cells have a significantly lower basal ER-free Ca^{2+} level and reduced ER

Ca^{2+} efflux following thapsigargin treatment (Figures 6F–6H). Apparent ER Ca^{2+} levels were restored to the baseline levels found in control cells by treatment with the Ca^{2+} ionophore ionomycin in the presence of 2 mM extracellular Ca^{2+}, indicating accurate and efficient D4ER FRET measurements under all conditions (Figures 6F and S7D).

Activation of SOCE in cells is characterized by formation of ER-plasma membrane junction puncta containing STIM1 and Orai1, as observed following 15-min thapsigargin treatment (Figure 6I, left panels). Under these conditions, VK_1 or ERGP alone did not affect formation of STIM1-Orai1 puncta, but the presence of γ-carboxylated ERGP significantly reduced formation of these protein complexes (Figures 6I and 6J). A FRET assay using YFP-Orai1 and STIM1-CFP was used as orthogonal validation of the impact of γ-carboxylated ERGP on formation of these complexes in living cells. Western blot analysis confirmed similar expression levels of the STIM1-CFP and YFP-Orai1 constructs in *ASPH*$^{-/-}$HEK293 cells under all conditions (Figure S7E), and live-cell imaging experiments confirmed that γ-carboxylated ERGP restrains formation of puncta co-expressing STIM1-CFP and YFP-Orai1 following 5-, 10-, and 15-min thapsigargin treatment (Figure 6K). Accordingly, these experiments revealed that the average corrected FRET signal following thapsigargin addition was significantly reduced in the presence of γ-carboxylated ERGP (Figures 6L–6N). These results suggest that, when γ-carboxylated, ERGP limits formation of STIM1-Orai1 complexes, thus restraining SOCE.

Ca^{2+} overfilling in *Ggcx*-deficient β cells causes impaired fasting hyperinsulinemia

We used *Ggcx*^{ff}*; Ins1-Cre* islets as a genetic model of decarboxylated ERGP in β cells to determine how γ-carboxylation of this protein affects Ca^{2+} homeostasis in these cells. Cytosolic Ca^{2+} flux was analyzed in partially dissociated islet cells from *Ggcx*^{ff}*; Ins1-Cre* and *Ins1-Cre* (control) mice by ratiometric live-cell imaging as above. SOCE was monitored with the protocol used for the HEK293 cells (Figure 6A) except that diazoxide, an opener of the ATP-sensitive K^+ channel, and verapamil, a voltage-gated Ca^{2+} channel (VGCC) blocker, were included in the buffered solution for the duration of imaging to prevent membrane depolarization and Ca^{2+} influx through the VGCC.[49] We first noticed that *Ggcx*^{ff}*; Ins1-Cre* β cells were characterized by higher cytosolic Ca^{2+} levels at baseline (Figures 7A and 7B). Moreover, SOCE expressed as absolute value or relative to baseline (ΔF) was increased in the same cells (Figures 7A and 7C). ER Ca^{2+} release was measured following treatment with a higher dose of thapsigargin (10 μM) and was found to be significantly higher in *Ggcx*^{ff}*; Ins1-Cre* β cells (Figure S7F). We also observed that the number of STIM1-containing puncta at steady state (i.e., 5 mM glucose) was more elevated in these cells in comparison with control islets, suggesting that γ-carboxylated ERGP restrains SOCE to maintain proper resting ER Ca^{2+} levels in β cells (Figures S7G–S7H).

Ca^{2+} flux in response to glucose confirmed higher basal cytosolic Ca^{2+} levels in *Ggcx*^{ff}*; Ins1-Cre* islets in comparison with *Ins1-Cre* islets (Figures 7D and 7E). Cytosolic Ca^{2+} levels after stimulation with 15 mM glucose or KCl were unchanged in the absence of carboxylated ERGP when normalized over the baseline, although they remained elevated in absolute value (Figures 7D and 7F). Altogether, these data suggest that ERGP γ-carboxylation is necessary to maintain Ca^{2+} homeostasis in primary β cells, mainly by

suppressing SOCE. In line with the data obtained with HEK293 cells, the increased SOCE present in *Ggcx^{ff}; Ins1-Cre* islet cells appears to result in increased basal cytosolic and ER Ca^{2+} levels.

Chronically elevated cytosolic Ca^{2+} in β cells has been linked to dysregulated insulin secretion and fasting hyperinsulinemia.[51,52] We next tested whether pharmacologically reducing cytosolic Ca^{2+} in *Ggcx^{ff}; Ins1-Cre* β cells could restore normal circulating fasting insulin levels *in vivo*. For this purpose, we selected verapamil, a VDCC blocker and well-characterized, US Food and Drug Administration (FDA)-approved drug. Verapamil treatment of *Ggcx^{ff}; Ins1-Cre* b-cells cultured with 11.1mM glucose *ex vivo* normalized their cytosolic Ca^{2+} within a few minutes (Figure 7G). In addition, verapamil provided in the drinking water for 5 days to mice fed a short-term HFD was sufficient to normalize the fasting insulin of *Ggcx^{ff}; Ins1-Cre* mice (Figure 7H). These results indicate that an increased cytosolic Ca^{2+} level in β cells is likely responsible for the fasting hyperinsulinemia observed *in vivo* in *Ggcx^{ff}; Ins1-Cre* mice maintained on an HFD (Figure 7I).

DISCUSSION

Link between the VK cycle and stress in β cells

Using conditional inactivation of *Ggcx* in mice and unique α-Gla antibodies, we established that the VK cycle is active in pancreatic islets and, more specifically, in β cells. Supporting a link between γ-carboxylation and β cell adaptation to stress, we found that glucose regulates γ-carboxylation activity and that VK_1 treatment can protect β cells from the deleterious effects of high glucose and ER stress. Together with the observation that mice lacking *Ggcx* in the pancreas or in β cells only failed to adapt their insulin secretion in response to short-term HFD feeding, our data suggest that the VK cycle could be part of a mechanism implicated in β cell survival and function under conditions of adaptation to metabolic stress. Therefore, we could speculate that lower VK intake or diminished γ-carboxylation activity could be a risk factor for development of diabetes when combined with nutrient excess in humans. In line with our findings, two recent large observational studies indicate that treatment with warfarin compared with a direct anticoagulant not targeting carboxylation does significantly increase the risk of new-onset diabetes in male and female patients with atrial fibrillation.[53,54]

ERGP γ-carboxylation as a regulator of β cell Ca^{2+} homeostasis

Our results identified ERGP as a γ-carboxylated protein present in islets and β cells. The data indicate that γ-carboxylated ERGP decreases formation of STIM1 and Orai1 puncta following ER Ca^{2+} store depletion, thereby partially inhibiting SOCE and reducing baseline cytosolic and ER Ca^{2+} levels. Conversely, decarboxylation of ERGP in *Ggcx^{ff}; Ins1-Cre* β cells was associated with increased cytosolic and ER Ca^{2+} levels at baseline and following SOCE. The impact of SOCE inhibition by γ-carboxylated ERGP on ER and cytosolic Ca^{2+} at steady state is consistent with the notion that SOCE is essential to maintain resting Ca^{2+} levels in the ER and cytosol, as reported previously by others.[46,47,55,56] We cannot exclude that γ-carboxylated ERGP directly controls ER Ca^{2+} levels, but we believe that it is unlikely, given that decreased ER Ca^{2+} levels will be expected to activate SOCE.[57] Rather, our data

suggest that γ-carboxylated ERGP restrains SOCE by acting directly or indirectly on the STIM1 conformational changes elicited by ER Ca^{2+} concentrations, consistent with our observations that SOCE and ER Ca^{2+} levels are increased in the absence of γ-carboxylation. Altogether the data imply that increased SOCE is the primary defect in *Ggcx^{ff};Ins1-Cre* β cells.

Junctate, whose luminal domain is identical to ERGP but has a different N-terminal cytosolic sequence, has been reported to interact with and regulate the SERCA2 pump and the inositol 1,4,5 trisphosphate receptors (IP3Rs), two ER membrane proteins controlling Ca^{2+} flux between the ER and the cytosol.[58,59] Whether γ-carboxylated ERGP also regulates Ca^{2+} homeostasis in β cells through a similar mechanism is currently unknown. It is important to note, however, that, in these earlier publications, junctate was studied in its decarboxylated form because VK was not included in the culture medium. It should also be noted that, because junctate and ERGP have distinct N-terminal cytosolic domains, these two proteins may affect cellular Ca^{2+} homeostasis through different mechanisms. Finally, because junctate mRNA was not detected in β cells, we did not further investigate the γ-carboxylation and function of this protein in this cell type.

Previous studies suggest that acute activation of Ca^{2+} flux between the ER and cytosol is critical for several β cell cellular processes, including survival and insulin secretion,[48,49,60] but that chronic stimulation of the Ca^{2+} signaling pathway can induce ER stress, β cell dysfunction, and death.[49,61,62] Our data show that the Ca^{2+} binding capacity of ERGP increases when γ-carboxylated and that this modification restrains SOCE, suggesting that γ-carboxylation could modulate ERGP ER Ca^{2+}sensing capacity. This process appears to be necessary to avoid Ca^{2+} overfilling and to maintain appropriate cytosolic and ER Ca^{2+} levels in β cells. Under conditions of chronically elevated intracellular Ca^{2+} levels, reducing Ca^{2+} entry would prove beneficial to prevent β cell dysfunction and diabetes progression. In humans, insufficient VK intake may therefore contribute to β cell dysfunction under conditions of β cell stress by reducing ERGP γ-carboxylation, thereby increasing the risk of T2D.

Fasting hyperinsulinemia as a driver of insulin resistance and T2D

It is noteworthy that mice lacking GGCX in the pancreas or only in β cells and fed an HFD for 7 days are characterized not only by reduced GSIS and increased blood glucose but also by increased fasting serum insulin and reduced insulin sensitivity. These observations are consistent with the notion that, under conditions of nutrient excess, chronic elevation of intracellular Ca^{2+} and ER stress in β cells can lead to uncontrolled hyperinsulinemia, which could ultimately result in peripheral insulin resistance.[51] There is a growing number of studies in rodents and humans suggesting that prolonged fasting insulin hypersecretion precedes and promotes insulin resistance and could be the initiating event of T2D.[1,3] Conversely, reducing insulin secretion can prevent insulin resistance, obesity, and fatty liver disease.[2,51] The metabolic phenotype of *Ggcx^{ff}; Ins1-Cre* mice following a short period of HFD feeding suggests that γ-carboxylated ERGP may be required to prevent uncontrolled insulin secretion by β cells in the context of nutrient excess and to preserve normal GSIS secretion.

ERGP as a VK-dependent protein

Since the discovery more than 45 years ago that a group of clotting factors is γ-carboxylated on specific Glu residues in a VK-dependent manner,[63] a total of 15 unique Gla proteins have been identified in mammals. They all share a relatively well-conserved “Gla domain” characterized by the presence of 3–12 γ-carboxylated Glu residues and two cysteines forming a disulfide bridge. While these proteins are either secreted or localized at the plasma membrane, ERGP and ASPH are ER-resident proteins, and their “Gla domain” possesses several unique features. First, the ASPH/ERGP GRD, with more than 190 a.a., is larger than the classic Gla domains, which are, on average, less than 50 a.a. long. Second, the ASPH/ERGP GRD does not contain a disulfide bridge, and the Gla residues are distributed in the N- and C-terminal regions instead of being clustered in the center. Third, ERGP and ASPH do not contain a sequence matching the GGCX substrate recognition sequence found in other Gla proteins. Together, these features suggest that ASPH and ERGP may define a distinct class of γ-carboxylated proteins in mammalian cells.

In conclusion, we propose here that VK-dependent γ-carboxylation is a post-translational modification regulating the capacity of β cells to adapt to stress. We also identify two mammalian VK-dependent proteins, ERGP and ASPH, and provide evidence that γ-carboxylation regulates β cell Ca^{2+} homeostasis through ERGP. Together, our findings extend the cellular and physiological function of VK-dependent γ-carboxylation and reveal how this pathway may interact with development of diabetes.

Limitations of the study

Although we show that γ-carboxylation is present in human islets, it remains to be established whether VK-dependent carboxylation is required to prevent Ca^{2+} overfilling in human β cells. In addition, the precise molecular mechanism by which γ-carboxylated ERGP restricts formation of the STIM1-Orai1 complex has not been determined here. Finally, we cannot exclude that ERGP may not be the sole γ-carboxylated protein mediating the effect of VK in β cells.

STAR⋆METHODS

RESOURCE AVAILABILITY

Lead contact—Further information and requests for resources and reagents should be directed to and will be fulfilled by the lead contact, Mathieu Ferron (mathieu.ferron@ircm.qc.ca).

Materials availability—All unique materials in this study may be made available upon request from the lead contact.

Data and code availability

- RNA-seq data have been deposited at GEO and are publicly available as of the date of publication. Accession number is GSE199319.

- The mass spectrometry proteomics dataset “Identification of vitamin K-dependent proteins in mouse liver by LC-MS/MS” has been deposited to the ProteomeXchange Consortium via the PRIDE partner repository[64] with the dataset identifier PXD032920 and https://doi.org/10.6019/PXD032920.
- The mass spectrometry proteomics dataset “Identification of gamma-carboxyglutamic acid residues in mouse ERGP by LC-MS/MS” have been deposited to the ProteomeXchange Consortium via the PRIDE partner repository[64] with the dataset identifier PXD032955 and https://doi.org/10.6019/PXD032955.
- This paper does not report original code.
- Any additional information required to reanalyze the data reported in this paper is available from the lead contact upon request.

EXPERIMENTAL MODEL AND SUBJECT DETAILS

Mice—*Ggcx*^{ff} mice were generated in our laboratory as described before,[13] and maintained on a C57BL/6J genetic background. These mice were bred to the *Pdx1-Cre* (B6.FVB-*Tg(Pdx1-cre)*^{6Tuv}/Nci; National Cancer Institute; Stock 01XL5)[65] or the *Ins1-Cre* (B6(Cg)-*Ins1*$^{tm1.1(cre)Thor}$/J; The Jackson Laboratory; Stock 026801)[66] lines to generate *Ggcx*^{ff}*; Pdx1-Cre* and *Ggcx*^{ff}*; Ins1-Cre* mice. β Cells were labeled with the tdTomato reporter gene by breeding the B6.Cg-*Gt(ROSA)26Sortm14(CAG-tdTomato)Hze*/J (Jackson Laboratory; stock 007914) mice to the *Ins1-Cre* strain. *Vkorc1*^{ff} and *Vkorc1l1*^{ff} mice were generated in our laboratory as described before,[13] bred to the *Pdx1-Cre* line to generate *Vkorc1*^{ff}*; Vkorc1l1*^{ff}*; Pdx1-Cre* mice and maintained on a C57BL/6J background. Other previously described mouse strains used in this study include *Vkorc1*$^{-/-}$*; APOE-Vkorc1l1*.[26] Male mice were used in all experiments and littermates with the appropriate genotypes always used as controls. Animals were housed at the IRCM in a pathogen-free facility on a 12h light/dark cycle and fed a normal chow diet (Teklad global 18% protein rodent diet; 2918; Envigo), unless otherwise specified. All animal use complied with the guideline of the Canadian Committee for Animal Protection and was approved by IRCM institutional animal care committee.

Human islets—Cadaveric human islets were obtained from the IsletCore at the Alberta Diabetes Institute from the University of Alberta (Edmonton, Alberta, Canada)[67] and from the Integrated Islet Distribution Program (IIDP) at City of Hope (Duarte, California, USA). Upon arrival, islets were handpicked and processed for experiments. When needed, human islets were cultured in DMEM (5mM glucose, 10% FBS, penicillin/streptomycin) in an incubator at 37°C, 5% CO_2. Detailed protocols for islet isolation and static glucose-stimulated insulin secretion are available in the protocols.io repository[68] and on the IIDP website (iidp.coh.org). Donor characteristics are described in Table S1. Islet isolation was approved by the Human Research Ethics Board at the University of Alberta (Pro00013094). All donors’ families gave informed consent for the use of pancreatic tissue in research. The IRCM Human Ethics committee approved human islets use.

Cell lines—Rat insulinoma cell line INS-1 832/3 (Millipore Sigma) was cultured in RPMI-1640 medium supplemented with 2mM L-Glutamine, 1mM sodium pyruvate, 10mM HEPES, 0.05 mM b-mercaptoethanol, 10% fetal bovine serum (FBS) and penicillin/streptomycin as previously described.[69] HEK293 cells (ATCC) were cultured in EMEM medium supplemented with heat-inactivated 10% FBS and penicillin/streptomycin. Cells were cultured at 37°C with 5% CO_2.

Generation of *ASPH*$^{-/-}$ HEK 293 cells by CRISPR-Cas9—HEK 293 cells were transfected with single guide RNA (sgRNA; Thermo Fisher) and recombinant *Streptococcus pyogenes* Cas9 protein (SpCas9; Synthego) using Lipofectamine CRISPRMAX Cas9 Transfection reagent (CMAX00001; Thermo Fisher) according to the manufacturer protocol. We selected a sgRNA (Assay ID: CRISPR671774_SGM; Target DNA Sequence: GGACATCTGTAG CTGTCGTT) matching a sequence in the exon 2 of the gene *ASPH* which is shared by all the isoforms encoded by this gene, including ASPH, junctate, junctin and ERGP proteins. Forty-eight hours after the transfection, cells were diluted and seeded in 96-wells plates to establish clonal lines. A total of ninety-six clones were screened by standard Sanger DNA sequencing of the targeted region and the sequence analyzed using the Inference of CRISPR Edits (ICE) Analysis tools of Synthego (https://ice.synthego.com/). Two clones with frameshift-inducing indel on all alleles of *ASPH* were selected and loss of expression of ASPH and ERGP confirmed by western blot experiment and by quantitative PCR (Figures S7A and S7B).

Rats and glucose infusions—Two-month-old male Wistar rats (Charles River, Saint-Constant, QC, Canada) underwent catheterization of the jugular vein for infusions and the carotid artery for sampling as described.[70] Animals were randomized into two groups receiving 0.9% saline (Baxter, Mississauga, ON, Canada; SAL) or 70% dextrose (McKesson, Montreal, QC, Canada; GLU) as described.[71] The glucose infusion rate was adjusted to maintain plasma glucose between 13.9 and 19.4 mmol/l throughout the 72h infusion. All procedures were approved by the Institutional Committee for the Protection of Animals at the Centre Hospitalier de l'Université de Montréal.

METHOD DETAILS

Mouse islet isolation, cell sorting and culture—Mice were anesthetized by intraperitoneal (i.p.) injection of a drug mixture of ketamine hydrochloride and xylazine, sacrificed via cervical dislocation and exsanguinated. The pancreatic duct was perfused with Liberase TL (Roche Applied Science) in Hank's balanced salt solution (HBSS) containing Ca^{2+}/Mg^{2+} and the inflated pancreas was excised and incubated at 37°C for 30 minutes with firm agitation at the 15-minute mark. The digested pancreas was then washed 4 times by decantation with HBSS containing 0.1% BSA and 20mM HEPES pH 7.4, and islets were isolated using Histopaque-1077 density gradient separation (Millipore Sigma). Islets were then transferred to culture medium (RPMI, 10% FBS, penicillin/streptomycin) and handpicked under a stereomicroscope (SteREO Discovery.V12; Zeiss).

Islets from *Ins1*$^{Cre/+}$; *Rosa26*$^{CAG\text{-}lox\text{-}stop\text{-}lox\text{-}tdTomato}$ mice were dissociated by incubating at 37°C for 2 minutes using 0.05% Trypsin-ETDA and pipetting. β Cells (Tom+) and the

other islet endocrine cells (Tom-) were sorted out based on tdTomato expression using the FACSAria III cell sorter (Becton Dickinson). Dead cells were excluded based on DAPI staining and only singlets were sorted. Cells were lyzed directly after sorting either in guanidium thiocyanate lysis solution for RNA extraction or in 1% triton lysis buffer for protein extraction.

INS-1 832/3 and islet treatments—To test the presence of γ-carboxylation, INS-1 832/3 cells and human islets were cultured in their respective culture medium containing either VK_1 (22μM; V3501; MilliporeSigma), warfarin (50μM; SC-204941; Santa Cruz Biotechnology), or vehicle during 3 days before analysis. To test the effect of glucose on γ-carboxylation, INS-1 832/3 cells, human islets and wild-type mouse islets were culture in their respective medium containing different concentration of glucose during 3 days before analysis. To test the protective effect of VK_1 on ER stress induced cell death, INS-1 832/3 cells were cultured with VK_1 (22μM) or vehicle for 48 hours before being cultured for 24 hours in medium containing 25mM glucose and thapsigargin (10, 20 and 40 nM). The dose of 22 μM (10 μg/ml) of VK_1 was selected based on previous reports showing that maximal γ-carboxylation of known Gla proteins was achieved with VK_1 concentration of >1–20 μM in cell culture.[72,73]

Metabolic analysis—For mice fed a regular chow diet, metabolic analysis was performed as follows. For intraperitoneal glucose tolerance tests (IPGTT), mice were fasted for 16 hours, and blood glucose levels were measured after fasting and at 15-, 30-, 60- and 120-minutes following i.p. injection of glucose (2g/kg of BW). To measure circulating insulin concentration following a bolus of glucose, tail vein blood was collected after a 16-hour fasting and at 15- and 30-minutes post-injection (i.p.) with glucose (3g/kg of BW). Serum insulin was measured using ELISA (Insulin ELISA mouse; Mercodia). Insulin tolerance test (ITT) was performed after 5 hours of fasting following i.p. injection of insulin (1U/kg; Humulin R, Lilly) and blood glucose was measured after fasting and 30-, 60-, 90- and 120-minutes post-injection.

For short high fat diet (HFD) feeding, 10-weeks old mice were fed either a lard-based diet (60% kcal from fat; TD.06414; Envigo) or an ingredient matched control diet (10% kcal from fat; TD.08806; Envigo) for 7 days, after which body weight, random fed blood glucose and metabolic tests were performed. For circulating insulin measurements, tail vein blood glucose was collected after 5 hours of fasting and at 15- and 30-minutes post-injection (i.p.) with glucose (2g/kg). Serum insulin was measured using ELISA and data represented in absolute value or as stimulation index (insulin concentration at 15 or 30 minutes / insulin concentration at fasting). For IPGTTs, tail vein blood glucose was measured after 5 hours of fasting and at 15-, 30-, 60- and 120-minutes post-injection with glucose (1.5g/kg). For oral glucose tolerance tests (OGTTs), tail vein blood glucose was measured after 5 hours of fasting and at 15-, 30-, 60- and 120-minutes post-gavage with glucose (1.5g/kg). For ITTs, tail vein blood glucose was measured after a 5-hour fasting and at 30-, 60-, 90- and 120-minutes post-injection (i.p.) with insulin (0.75U/kg). Homeostatic model assessment of insulin resistance (HOMA-IR) was calculated as follows: Fasting glucose (mM) × Fasting insulin (μU/mL)/22.5.[74] When indicated, following 7 days of HFD feeding, verapamil

(V4629, Sigma) was added to the drinking water (1mg/mL) of the mice for 5 days while fed an HFD.

O_2 consumption, CO_2 release, food intake and physical activity were analyzed using an 8-chamber Promethion Continuous Metabolic System (Sable Systems International) as before[75]. Briefly, after a 48-hour acclimation period, data were collected for 96 hours. Energy expenditure (kcal/hour) was calculated by indirect calorimetry using the following formula: $60 \times (0.003941 \times VO_2$ (ml/min) $+ 0.001106 \times VCO_2$ (ml/min)). Physical activity was measured as beam breaks for the x-, y- and z-axis using infrared beams connected to the system.

***Ex vivo* glucose-stimulated insulin secretion (GSIS)—**Islets from *Ggcx^{ff}; Pdx1-Cre* and *Pdx1-Cre* mice were isolated and left in culture medium (RPMI, 10% FBS, penicillin/streptomycin) for recovery for 40 hours. Islets were hand-picked and quickly washed in Krebs-Ringer bicarbonate HEPES (KRBH) buffer (114mM NaCl, 2.5mM $CaCl_2$, 1.2mM KH_2PO_4, 4.7mM KCl, 1.16mM $MgSO_4$, 25.5mM $NaHCO_3$, 10mM HEPES and 0.1% fatty acid free BSA, pH 7.35) containing 5.6mM glucose, and then pre-incubated two times for 1 hour at 37°C. Groups of 10 similarly sized islets were transferred to microtubes containing 5.6mM glucose KRBH and incubated for 1h at 37°C. Islets were then incubated in KRBH buffer containing 11.1mM glucose, followed by KRBH buffer containing 16.7mM glucose, each incubation for 1 hour at 37°C. After each incubation, supernatant was collected and at the end of the protocol, islets were lyzed in 0.18N HCl, 75% EtOH extraction buffer. Insulin was measured in the different fractions by ELISA (Mercodia). Islets insulin content was used to normalize insulin secretion.

Pancreas immunohistochemistry, immunofluorescence and insulin content —Pancreases were weighed and fixed in 10% formalin for 24 hours at room temperature, embedded in paraffin and sectioned at 5μm. For immunohistochemistry and immunofluorescence experiments, rehydration was followed by an antigen retrieval step (sub-boiling for 10 minutes in 10mM sodium citrate pH 6.0).

For β cell mass quantifications, insulin was detected using rabbit anti-insulin antibodies (1:200, sc-9168; Santa Cruz Biotechnology), Vectastain Elite ABC-peroxidase kit (Vector Laboratories; PK-6101) and NovaRED Substrate Kit (Vector Laboratories; SK-4800) following manufacturer's instructions. Pancreas tissue was counterstained using Mayer's hematoxylin and histomorpho-metric analyses were performed using the OsteoMeasure Analysis System (Osteometrics). β Cell mass was calculated as follows: β cell area (%) × pancreas weight (mg) / 100.

For immunofluorescence, blocking was performed in PBS containing 5% normal donkey serum and 0.3% Triton for 1 hour at room temperature. Sections were then incubated with antibodies diluted in PBS, 1% BSA and 0.1% Triton, first with goat anti-insulin antibodies (sc-7839; Santa Cruz Biotechnology) and rabbit anti-A/E-GRD antibodies (generated in our laboratory, see below) over-night at 4°C, and second with Alexa-Fluor 594- conjugated donkey anti-goat (705-585-147; Jackson Immunoresearch Laboratories) and Alexa-Fluor 488-conjugated donkey anti-rabbit (711-545-152; Jackson Immunoresearch Laboratories)

antibodies for 1 hour at room temperature. Specificity of anti-A/E-GRD antibodies was assessed by competition with recombinant 6XHIS-A/E-GRD protein (25μg/mL) during incubation with the primary antibodies. Nuclei were stained with DAPI. Volocity 6.0 quantitation module was used to threshold for and select Insulin$^+$ cells and to determine the intensity of the A/E-GRD signal in Insulin$^+$ areas.

For apoptosis detection, the Click-iT Plus TUNEL Assay kit (C10617; Invitrogen) was used following manufacturer's instructions except the proteinase K treatment was replaced by a 10-minute incubation in citrate buffer. Goat anti-insulin antibodies (sc-7839; Santa Cruz Biotechnology) and Alexa-Fluor 594- conjugated donkey anti-goat antibodies (705-585-147; Jackson Immunoresearch Laboratories) were used as described above. Nuclei were stained with DAPI. Insulin$^+$ TUNEL$^+$ cells were detected using the automated DM5500B fluorescence microscope (Leica) with a Retiga EXi (QImaging) and 40X objective. Volocity 6.0 quantitation module was used to threshold for and count Insulin$^+$ cells with TUNEL$^+$ nuclei.

For pancreatic insulin content measures, each pancreas was weighed and homogenized in an acid-ethanol buffer (1.5% HCl; 70% EtOH) after overnight fasting and 2 hours of refeeding. Samples were neutralized using 1M Tris-HCl pH 7.5 (1:1) and insulin measured by ELISA (Mercodia). Insulin content was normalized to the pancreas weight.

RNA isolation and qPCR—For mouse and human islets gene expression analysis, 20–40 handpicked islets per mouse or donor were lyzed in guanidium thiocyanate lysis solution, and tRNA (20ug) was added before total RNA was isolated as described.[76] Samples were then treated with DNaseI (18068015; Invitrogen), and mRNA reversed transcribed using M-MLV reverse transcriptase (28025013; Invitrogen) and random hexamers and oligo dT primers. Relative gene expression was quantified using PowerUp SYBR Green Master Mix (A25741; Applied Biosystems) and ViiA7 Real-Time PCR System (Applied Biosystems).

DNA constructs and transfections—Mouse ASPH-3XFLAG and ERGP-3XFLAG plasmids were generated by PCR amplification using pENTR223.1-ASPH (Clone ID: BC166658; Transomic Technologies) as a template and cloning in the HindIII and BamHI restriction sites of the p3XFLAG-CMV-14 expression vector (MilliporeSigma). ASPH-3XFLAG and ERGP-3XFLAG deletion mutants were generated by PCR using Q5 High Fidelity DNA polymerase (M0491; NEB) and primers extending in opposite directions and flanking the region to be deleted. ERGP DNA fragments containing glutamic acid to aspartic acid point mutations were synthesized (Genscript) and cloned into ERGP-3XFLAG plasmid via an internal StuI site and the 3′ BamHI site. Mouse Orai-HA was generated in two steps. First, the 3′ section of Orai1 ORF was cloned from pCMV-SPORT6-Orai1 (BC023149; Transomic Technologies) in the EcoRI and XbaI restriction sites of a pcDNA3.1-Myc-His B expression vector with an HA tag. The missing 5′ section of Orai1 ORF was cloned from mouse osteoblast cDNA in the EcoRI and Orai1 internal ApaI restriction sites. Mouse pcDNA3.1-Stim1-Myc plasmid was obtained from Addgene (17732).[77] Using the above-mentioned constructs as template, STIM1-CFP and YFP-Orai1 were inserted into the pcDNA3.1-Myc-His B vector using Gibson assembly. pcDNA-D4ER plasmid was previously described and obtained from Dr. Diana Pendin.[50]

HEK293 cells were transfected with “tagless” pCDNA3.1-GGCX and pCDNA3.1-VKORC1 to ensure maximal γ-carboxylation, and with the indicated plasmids using Lipofectamine 2000 transfection reagent (11668019; Invitrogen) following manufacturer’s instructions. Six hours post-transfection, medium was changed and VK_1 (22μM) or warfarin (50μM) was added when specified. Generation of a clonal cell line stably expressing ERGP-3XFLAG was generated via transfection of HEK293 cells with the pERGP-3XFLAG-CMV-14 plasmid previously linearized by digestion with ScaI. Cells with integration of the plasmid were selected using G418 antibiotics and isolated colonies were expanded. ERGP expression was assessed by western blot using anti-FLAG antibodies and immunofluorescence confirming clonality.

Ca^{2+} overlay—HEK293 cells stably expressing mouse ERGP-3XFLAG, and transfected with GGCX and VKORC1, were cultured in the presence of either VK_1 (22μM) or warfarin (10μM). Purified γ-carboxylated and uncarboxylated ERGP-3XFLAG proteins were resolved by SDS-PAGE, transferred to a nylon membrane and cross-linked with 0.5% glutaraldehyde. The membrane was quenched with 50mM glycine and washed 3 times with binding buffer containing 60mM KCl, 5mM $MgCl_2$, 10mM imidazole-HCl, pH 6.8, and then incubated with radiolabelled binding buffer containing 8.8μM $^{45}CaCl_2$ (PerkinElmer) for 1 hour, washed with distilled H_2O and dried. Radioactivity was captured by a storage phosphor screen and detected by a laser scanner imaging system (Typhoon FLA 9500; Cytiva).

Generation of rabbit polyclonal anti-ASPH/ERGP-GRD (anti-A/E-GRD) antibodies—Rabbit ERGP ER luminal domain anti-serum was generated by immunizing rabbits with a 6XHIS-tagged protein containing amino acid 85–310 of ERGP (MediMabs). Antibodies specific to the glutamic acid rich domain (GRD) were affinity purified using a GST-tagged protein corresponding to the GRD. The specificity of the antibody towards the GRD of ERGP and ASPH was tested by western blot.

Immunoprecipitation and western blot—Cells or tissues were homogenized in lysis buffer containing 20mM Tris-HCl (pH 7.5), 150mM NaCl, 1mM EDTA (pH 8.0), 1mM EGTA, 2.5mM NaPyrophosphate, 1mM b-glycerophosphate, 10mM NaF, 1% Triton, 1mM phenylmethylsulfonyl fluoride (PMSF) and protease inhibitors (4693132001; Roche Diagnostics). For anti-Gla immunoprecipitation, 200μg of protein extracts was incubated with 10μg of rabbit anti-Gla antibodies overnight with rotation at 4°C followed by 3 hours incubation with Protein A-Agarose beads (11719408001; Roche Diagnostics) and washed 4 times with lysis buffer. Immunoprecipitated proteins were heated at 70°C in Laemmli buffer for 10 minutes before resolving on a 7.5% polyacrylamide Tris-Glycine gels. Proteins were detected using standard western blot procedures with rabbit anti-GGCX (16209–1-AP; ProteinTech) or rabbit anti-A/E antibodies generated in our laboratory (see above). For anti-A/E-GRD IP, the same procedure was followed. FLAG-tagged proteins were immunoprecipitated from 100μg of protein extracts using anti-FLAG agarose beads (A2220; MilliporeSigma) incubated for 2 hours with rotation at 4°C. Densitometry analyses were performed with the Image Lab software (version 5.0; Bio-Rad Laboratories).

Other antibodies used for western blot in this study include rabbit anti-VKORC1 generated in our laboratory and previously reported,[13] rabbit anti-cleaved Caspase-3 (9661; Cell Signaling), rabbit anti-phospho(Ser139)-Histone H2A.X (9718; Cell Signaling), rabbit anti-phospho(S724)-IRE1 (ab124945, Abcam), rabbit anti-GRP78/BIP (11587–1-AP, Proteintech), rabbit anti-GFP (50430–2-AP, Proteintech), mouse anti-β-Actin (A1978; MilliporeSigma), rabbit anti-GAPDH (5174; Cell Signaling), mouse anti-Myc (2276; Cell Signaling), rabbit anti-HA (3724; Cell Signaling), mouse anti-FLAG (F1804; MilliporeSigma) and rabbit anti-FLAG (14793; Cell Signaling). To detect VKORC1, cleaved Caspase-3 and p(Ser139)-Histone H2A.X, proteins were resolved on 10% polyacrylamide Tris-Tricine gels.

Ca^{2+} live-cell imaging in $ASPH^{-/-}$ HEK293 and islets—$ASPH^{-/-}$ HEK 293 cells were transfected with 0.5μg GGCX, 0.5μg VKORC1, 0.44μg STIM1-Myc, 0.22μg Orai1-HA, 0.33μg ERGP-3XFLAG or p3XFLAG-CMV-14 empty vector as indicated in 35mm culture dishes and the next day cells were plated on poly-L-lysine (P1274; MilliporeSigma) coated glass coverslips (18mm diameter, #1.5 thickness; 72290–08; Electron Microscopy Sciences). Coverslips were coated with 0.1mg/mL poly-L lysine in sterile ddH_2O at room temperature for 1 hour, before being washed three times with sterile ddH_2O and left to dry for 2 hours. $ASPH^{-/-}$ HEK 293 cells were loaded with 5μM Fluo-4 AM (F14201; Invitrogen) and 2.5μM Fura Red AM (F3021; Invitrogen) in a HEPES-buffered saline solution (HBSS; 120mM NaCl, 5mM KCl, 0.8mM $MgSO_4$, 2mM $CaCl_2$, 10mM Glucose, 20mM HEPES, pH 7.4) containing 0.02% pluronic F-127 (P6866; Invitrogen) at 37°C for 30 minutes. Cells were then washed twice with HBSS and incubated for an additional 30 minutes at 37°C to allow complete de-esterification of intracellular AM esters. Ca^{2+} imaging was performed in Ca^{2+} free HBSS containing 1mM EGTA. Baseline measurements (F0) were recorded for 120 seconds before ER Ca^{2+} stores were depleted by adding thapsigargin (final 1μM) and SOCE was triggered by adding $CaCl_2$ (final [Ca^{2+}] 2mM) 420 seconds after starting recording. For measurements using the D4ER Ca^{2+} probe, $ASPH^{-/-}$ HEK293 cells were transfected with 0.2μg D4ER, 0.4μg GGCX, 0.4μg VKORC1, 0.44μg STIM1-Myc and 0.22μg Orai1-HA and 0.33μg ERGP-3XFLAG or p3XFLAG-CMV-14 empty vector. The cells were equilibrated in HBSS for 45 minutes at 37°C before being imaged in Ca^{2+} free HBSS containing 1mM EGTA. Baseline measurements were recorded for 600 seconds before ER Ca^{2+} stores were depleted by adding thapsigargin (final 1μM). The Ca^{2+} ionophore ionomycin (final 3μM) and $CaCl_2$ (final [Ca^{2+}] 2mM) were added 1200 seconds after starting recording. Imaging of HEK293 cells was performed at 37°C.

Isolated mouse islets were semi-dispersed by digestion with 0.025% Trypsin-ETDA for 1 minute followed by up and down pipetting then transferred to culture medium (RPMI, 10% FBS, penicillin/streptomycin) containing 22μM VK_1. Semi-dispersed islets enclosed in 200 μL droplets (corresponding to approximately 100 islets) were plated on glass coverslips and allowed to attach for 30 min at 37°C, before adding 1mL of culture medium for over-night recovery. Islet cells were then loaded with 5μM Fluo-4 AM and 2.5μM Fura Red AM in KRBH buffer (114mM NaCl, 1.2mM KH_2PO_4, 4.7mM KCl, 1.16mM $MgSO_4$, 25.5mM $NaHCO_3$, 2.5mM $CaCl_2$, 5mM Glucose, 20mM HEPES, 0.2% fatty acid free bovine serum albumin [BSA]) for 30 minutes at room temperature. Baseline fluorescence

ratio (F0) was measured for 90 seconds and response to 15mM glucose was recorded during 90–1700 seconds before KCl concentration was raised to 30mM. SOCE in islet cells was measured as described above for HEK293 but in KRBH buffer containing 200μM diazoxide (D9035; MilliporeSigma), an opener of the ATP sensitive K^+ channel in β cells, and 10μM verapamil (V4629; Millipore Sigma), a voltage gated Ca^{2+} channel blocker, for the duration of imaging. In other experiments, the effect of verapamil on cytosolic Ca^{2+} levels of semi-dispersed islets was measured as described above, but in KRBH buffer containing 11mM glucose to mimic *in vivo* conditions. The semi-dispersed islets were first imaged for 600 seconds following vehicle (DMSO) treatment, then were imaged for an additional 600 seconds following treatment with 50μM verapamil. Imaging for islets was performed at 32°C and 5% CO_2 enrichment.

Imaging was performed on a confocal rotary disk inverted microscope from Zeiss equipped with a Yokogawa CSU-1 module using a 20X objective. The microscope stage contained a conduction heater and was enclosed in an incubator to maintain cells at the desired temperature and CO_2 percentage. Fluo-4 was excited with a 488nm laser and emission was recorded at 509nm (ZEN blue software). Laser power was set to 5%, exposure to 250ms, and EM gain to 500. One image was taken every 5 seconds. Fura Red was excited with a 488nm laser and emission was recorded at 660nm. Laser power was set to 20%, exposure to 500ms, and EM gain to 750. One image was taken every 5 seconds. D4ER reports ER Ca^{2+} level via FRET between its CFP and Citrine domains, which come into closer proximity following Ca^{2+} binding of its D4 and calreticulin domains. To record the CFP donor signal, D4ER was excited with a 405nm laser then emission recorded at 475nm. To record the FRET signal from Citrine, D4ER was excited with a 405nm laser then emission recorded at 524nm. Laser power was set to 20%, exposure to 500ms, and EM gain to 750 to record CFP. Laser power was set to 20%, exposure to 500ms, and EM gain to 500 to record Citrine FRET.

Quantification was performed using Fiji[78]. Timelapses were 16-bit greyscale image stacks saved as Carl Zeiss Image data format files. Individual cells or islet clusters were selected as freehand selections to generate regions of interest (ROI). The mean gray value of each ROI was then measured for each image (1 per 5 seconds) for each channel (Fluo-4/Fura Red or Citrine/CFP). Cells that did not stay attached during the entire protocol were excluded from analysis. Fluo-4 fluorescence intensity was divided by Fura Red intensity to generate a ratiometric measurement of cytosolic Ca^{2+} as previously described.[79] Similarly, the intensity of the FRET signal from Citrine was divided by the CFP intensity to generate a ratiometric measurement of ER Ca^{2+} for the experiments using the D4ER probe as previously described.[50] The FRET-Citrine/CFP ratio was then normalized to the mean of the first 100 seconds recorded for the vehicle condition (i.e., without VK_1 and without ERGP) and represented as % of vehicle. A total of n=54–130 $ASPH^{-/-}$ HEK 293 cells were averaged together for each experiment for cytosolic or ER Ca^{2+} measurements, and n=9–14 independent experiment per condition were analyzed. In semi-dispersed islet imaging experiments, 82–240 islet cell clusters were averaged for each experiment, and n=7–8 independent experiment per condition were analyzed.

STIM1/Orai1 puncta quantification by immunofluorescence—*ASPH*$^{-/-}$ HEK293 cells were transfected with GGCX, VKORC1, STIM1-myc, and Orai1-HA and ERGP-3XFLAG or p3XFLAG-CMV-14 empty vector, and plated on poly-L-lysine coated glass coverslip as detailed in the Ca^{2+} live-imaging section. Two days later, cells were equilibrated in HBSS for 45 minutes and treated with 1μM thapsigargin for 15 minutes in Ca^{2+} free HBSS containing 1mM EGTA. Cells were then fixed in 4% paraformaldehyde in PBS for 15 minutes at room temperature and washed 3 times with PBS. Cells were stained using mouse anti-Myc (Cell Signalling; 2276) and rabbit anti-HA (Cell Signalling; 3724) antibodies as detailed in the immunofluorescence section and imaged with a 63x objective.

Quantification of puncta was performed using the Volocity 6.0 quantitation module. Puncta were determined by adjusting an intensity threshold and including only objects measuring between 0.1-and 1.0μm^2. Saturated pixels were excluded from quantification. STIM1/Orai1 co-expressing puncta in *ASPH*$^{-/-}$ HEK293 cells were defined as areas of overlapping STIM1 and Orai1 expression in objects between 0.1–1.0μm^2 in surface area. On average a cell contains 0–120 puncta in the absence of thapsigargin and 15–413 puncta following thapsigargin treatment. The number of STIM1/Orai1 colocalized puncta per cell was normalized to the cell area in μm^2 (n=27–34 cells per condition, from 3 independent experiments). Islet clusters stained for STIM1 (rabbit anti-STIM1; 5668; Cell Signaling) contained on average 0–57 puncta at steady state (KRBH buffer with 5mM glucose). The number of STIM1 puncta per islet cluster was normalized to the cluster area in μm^2 (n=116–183 islets clusters per condition, from 2 independent experiments).

STIM1/Orai1 FRET measurements—*ASPH*$^{-/-}$ HEK293 cells were transfected with 0.4μg GGCX, 0.4μg VKORC1, 0.44μg STIM1-CFP, 0.42μg YFP-Orai1 and 0.33μg ERGP-3XFLAG or p3XFLAG-CMV-14 empty vector and plated on poly-L-lysine coated glass coverslips the next day as detailed in the Ca^{2+} live-cell imaging section. Two days later, cells were washed twice with HBSS and imaged for 120 seconds before 1μM thapsigargin and 3mM EGTA was added to deplete ER Ca^{2+} stores and chelate extracellular Ca^{2+}. Transfection were optimized to get <2-fold difference between STIM1-CFP and YFP-Orai1 expression levels. Images were recorded every three seconds with the 63X objective of a confocal rotary disk inverted microscope as described in the Ca^{2+} live-cell imaging section.

STIM1-CFP was excited with a 405nm laser and emission was recorded at 475nm. Laser power was set to 20%, exposure to 750ms, and EM gain to 750. YFP-Orai1 was excited with a 488nm laser and emission was recorded at 524nm. Laser power was set to 10%, exposure to 250ms, and EM gain to 500. FRET signal was excited with the 405nm laser and emission was recorded at 524nm. Laser power was set to 20%, exposure to 500ms, and EM gain to 500.

Quantification was performed using Fiji[78] as previously described[80,81]. Time lapse images were 16-bit greyscale image stacks saved as Carl Zeiss Image data format files. Each timepoint contained three images representing the CFP, YFP, and FRET channels. Individual cells were selected manually using the freehand ROI selection tool. Identical ROIs were used across timepoints and channels for each time lapse. An ROI containing no cells was

also selected on each time lapse and used to subtract the background value of each channel. For each imaging experiment, cells transfected with STIM1-CFP or YFP-Orai1 alone were used to calculate bleed-through of the CFP or YFP signals into the FRET channel. The bleed-through coefficient for CFP (A) and YFP (B) were individually calculated, using linear regression of CFP or YFP intensity in their respective channels compared to the signal in the FRET channel.

Corrected FRET signal was defined as follows:

$$FRET_{corr} = FRET - ([\ A \times CFP\ ] + [\ B \times YFP\ ])$$

Where FRET is the fluorescent intensity at 524nm from the FRET channel, CFP is the fluorescent intensity at 475nm from the CFP channel, YFP is the fluorescent intensity at 524nm from the YFP channel, A is the CFP-FRET bleed-through coefficient determined by imaging CFP only cells, and B is the YFP-FRET bleed-through coefficient determined by imaging YFP only cells. Corrected FRET was divided by CFP intensity to control for transfection efficiency ($FRET_{corr}$/CFP). A total of n=37–61 cells, from 3 independent experiments, were averaged together for each condition.

Area under the curve (AUC) of $FRET_{corr}$/CFP traces were calculated with baseline AUC subtraction.

RNA-sequencing—Total RNA from islets was extracted using the RNeasy Plus Mini Kit (74134; Qiagen) following manufacturer's instructions (n=4 for each genotype). RNA integrity was evaluated using the 2100 Bioanalyzer system (Agilent) and samples with RIN >7.5 were used. From 1μg of total RNA, poly(A)+ transcripts were enriched using the NEBNext Poly(A) Magnetic isolation module (E7490; NEB) and libraries prepared using the KAPA stranded RNA-seq library preparation kit (KR0934; Roche Diagnostics) and the TruSeq DNA library Prep LT kit (Illumina) according to the manufacturer's procedures. Clustering of the equimolar libraries in the flowcell was performed using the HiSeq PE cluster kit v4 cBot (PE-401–4001; Illumina) and the cBot cluster generation system (Illumina). Sequencing was performed at the Génome Québec Innovation Center using the Illumina HiSeq 2500 system (average of 56 million paired end reads (PE50) per sample). The quality of the raw reads was assessed with FASTQC v0.11.8. After examining the quality of the raw reads, no trimming was deemed necessary. The reads were aligned to the GRCm38 genome with STAR v2.7.6a with more than 87% of reads uniquely mapped. Raw counts were computed using FeatureCounts v1.6.0 based on Ensembl mouse reference genome v101. Differential expression was performed using the DESeq2 R package and 319 differentially expressed genes (DEGs) were obtained using p-adjusted %0.05. Gene set enrichment and gene network analyses were performed using StringDB (https://string-db.org/)[82] interrogating Biological Process (Gene Ontology), KEGG Pathways and Annotated Keywords (UniProt). Enrichment was considered significant if the false discovery rate was <0.05 and only networks of 800 or fewer genes were considered for the analysis. Previously published transcriptomic analysis of islets from pre-diabetic (5-weeks old C57BL/6 mice fed a HFD for 8 weeks) or diabetic (8-weeks old *Lepr*$^{db/db}$ and 7-weeks old *Ire1a*^{ff}*; Ins2-Cre*$^{ERT/+}$) mouse models,[31–33] were downloaded directly from the publications

or from GEO (https://www.ncbi.nlm.nih.gov/geo/). Up-regulated and down-regulated genes for each model were selected using different p-adjusted values to limit the variability in the total number of genes included in each list: $p < 0.05$ for *Lepr*$^{db/db}$, $p < 0.01$ for HFD and $p < 0.001$ for *Ire1a*^{ff}; *Ins2-Cre*$^{ERT/+}$. Overlap between the various transcriptomes was next determined using jvenn (http://jvenn.toulouse.inra.fr/app/example.html).[83] The statistical significance between each pair of comparisons was computed using an online tool (http://nemates.org/MA/progs/overlap_stats.html).

Identification of carboxylated proteins by LC-MS/MS—Livers from 5-day old WT and *Vkorc1*$^{-/-}$ mice, or INS-1 832/3 cells cultured with VK_1, 25mM glucose with or without 20nM thapsigargin, were homogenized in lysis buffer and carboxylated proteins immunoprecipitated as described above followed by three washes with 50mM ammonium bicarbonate. Immunoprecipitated proteins were then digested on-bead with trypsin at 37°C for 18 hours using 0.25ug of Sequencing grade trypsin (Promega). The samples were then reduced with 9 mM dithiothreitol at 37°C for 30 minutes and, after cooling for 10 minutes, alkylated with 17 mM iodoacetamide at room temperature for 20 minutes in the dark. The supernatants were acidified with trifluoroacetic acid and cleaned from residual detergents and reagents with MCX cartridges (Waters Oasis MCX 96-well Elution Plate) following the manufacturer's instructions. After elution in 10% ammonium hydroxide /90% methanol (v/v), samples were dried with a Speed-vac, reconstituted under agitation for 15 min in 11 µL of 2%ACN-1%FA and 2.4% of each sample was loaded into a 75 µm i.d. × 150 mm Self-Pack C18 column installed in the Easy-nLC II system (Proxeon Biosystems). The buffers used for chromatography were 0.2% formic acid (buffer A) and 90% acetonitrile/ 0.2% formic acid (buffer B). Peptides were eluted with a two slopes gradient at a flowrate of 250 nL/min. Solvent B first increased from 2 to 44% in 100 min and then from 44 to 88% B in 20 min. The HPLC system was coupled to Orbitrap Fusion mass spectrometer (Thermo Scientific) through a Nanospray Flex Ion Source. Nanospray and S-lens voltages were set to 1.3–1.7 kV and 50 V, respectively. Capillary temperature was set to 225°C. Full scan MS survey spectra (m/z 360–1560) in profile mode were acquired in the Orbitrap with a resolution of 120,000 with a target value at 3e5. The 25 most intense peptide ions were fragmented in the HCD cell and analyzed in the linear ion trap with a target value at 2e4 and a collision energy at 29. Target ions selected for fragmentation were dynamically excluded for 30 sec after 2 MS/MS events.

The peak list files were generated with Proteome Discoverer (version 2.3) using the following parameters: minimum mass set to 500 Da, maximum mass set to 6000 Da, no grouping of MS/MS spectra, precursor charge set to auto, and minimum number of fragment ions set to 5. Protein database searching was performed with Mascot 2.6 (Matrix Science) against the UniProt Mus Musculus protein database. The mass tolerances for precursor and fragment ions were set to 10 ppm and 0.6 Da, respectively. Trypsin was used as the enzyme allowing for up to 1 missed cleavage. Cysteine carbamidomethylation was specified as a fixed modification, and methionine oxidation, glutamic acid carboxylation and phosphorylation S/T/Y as variable modifications. Data interpretation was performed using Scaffold (version 4.8) using a peptide threshold of 80%, a protein threshold of 95% and one peptide minimum. We considered a protein as being carboxylated when the average

exclusive spectrum count in WT samples was at least double of the *Vkorc1*$^{-/-}$ samples. To minimize the potential identification of proteins non-specifically binding the anti-Gla antibodies or the agarose-beads, we excluded proteins with more than 2 exclusive spectrum counts in the *Vkorc1*$^{-/-}$ samples or with a difference of less than 2 between the WT and *Vkorc1*$^{-/-}$ samples.

Identification of carboxylated residues in ERGP by LC-MS/MS—HEK293 cells stably expressing mouse ERGP-3XFLAG were cultured in the presence of either VK_1 (22μM) or warfarin (10μM) for at least 2 weeks, and carboxylated and uncarboxylated ERGP-3XFLAG were purified with anti-FLAG agarose beads (A2220; MilliporeSigma). On-bead proteins were first diluted in 2M Urea/50mM ammonium bicarbonate, and on-bead chymotrypsin digestion was performed overnight at 37°C. The supernatants were acidified with trifluoroacetic acid and cleaned from residual detergents and reagents with MCX cartridges (Waters Oasis MCX 96-well Elution Plate) following the manufacturer's instructions. After elution in 10% ammonium hydroxide /90% methanol (v/v), samples were dried with a Speed-vac, reconstituted under agitation for 15 min in 11 μL of 2%ACN-1%FA and loaded into a 75 μm i.d. × 150 mm, Self-Pack C18 column, installed in the Easy-nLC II system (Proxeon Biosystems). Peptides were loaded on-column and eluted with a two-slope gradient at a flow rate of 250 nL/min. Solvent B first increased from 1 to 32% in 86 min and then from 32 to 82% B in 22 min. The HPLC system was coupled to Orbitrap Fusion mass spectrometer (Thermo Scientific) through a Nanospray Flex Ion Source. Nanospray and S-lens voltages were set to 1.3–1.8 kV and 50 V, respectively. Capillary temperature was set to 250 °C. Full scan MS survey spectra (m/z 320–1520) in profile mode were acquired in the Orbitrap with a resolution of 120,000 with a target value at 5e5. The most intense peptide ions were fragmented by ETD, CID and ETciD and analysed in the linear ion trap with a target value at 1e4. The peptide ion fragmentation parameters were as follow: a reaction time of 120 ms, a reagent target of 2.0e5 and a maximum reagent injection time of 200 ms for ETD, a normalized collision energy of 32% for CID, calibrated charge dependent ETD parameters and normalized supplemental activation at 18% for ETciD. The duty cycle was set to 4 seconds and target ions selected for fragmentation were dynamically excluded for 30 sec after 2 MS/MS scan events. Uncarboxylated bacterially produced His-tagged ERGP was digested in-solution with chymotrypsin in the aforementioned conditions.

The peak list files were generated with Proteome Discoverer (version 2.1 or 2.4) using the following parameters: minimum mass set to 500 Da, maximum mass set to 6000 Da, no grouping of MS/MS spectra, precursor charge set to auto, and the minimum number of fragment ions set to 5. Protein database searching was performed with Mascot 2.6 (Matrix Science) against a user-defined mouse ERGP database. The mass tolerances for precursor and fragment ions were set to 10 ppm and 0.6 Da, respectively. A semi-specific search was performed using chymotrypsin as the enzyme allowing for up to 1 missed cleavage. Methionine oxidation and carboxylation of glutamic acid were specified as variable modifications. Data interpretation was performed using Scaffold (version 4.8).

QUANTIFICATION AND STATISTICAL ANALYSIS

All the statistical details of experiments can be found in the figure legends. Statistical analyses were performed using GraphPad Prism software (version 9.3.1). Results are given as means ± SEM. For single measurement, unpaired, 2-tailed Student's *t* test was used. Grouped analysis was performed using one-way ANOVA, followed by Bonferroni's multiple comparisons test. For repeated measurements (metabolic tests), two-way ANOVA followed by Bonferroni's post tests were used. Linear correlations were analyzed using Pearson's correlation. In all figures, $*P < 0.05$; $**P < 0.01$; $***P < 0.001$. All experiments were repeated at least 3 times or performed on at least 3 independent animals.

Supplementary Material

Refer to Web version on PubMed Central for supplementary material.

ACKNOWLEDGMENTS

We thank Dr. K. Suh for providing the B6.Cg-Gt(ROSA)26Sor$^{tm14(CAG-tdTomato)Hze}$/J mice, Dr. D. Pendin and Dr. T. Pozzan for providing the D4ER probe, and Dr. G. Karsentyfor critical reading of the manuscript. We alsothank the staff of the IRCM Core Facilities for technical support. Human islets for research were provided by the Alberta Diabetes Institute IsletCore at the University of Alberta in Edmonton (http://www.bcell.org/adi-isletcore.html) with the assistance of the Human Organ Procurement and Exchange (HOPE) program, Trillium Gift of Life Network (TGLN), and other Canadian organ procurement organizations. When indicated, human pancreatic islets were provided by the NIDDK-funded Integrated Islet Distribution Program (IIDP) (RRID: SCR_014387) at City of Hope, NIH grant #2UC4DK098085. This work was supported by funding from the Canada Research Chair program (to M.F.), Diabetes Canada (OG-3-21-5599-MF to M.F.), Diabète Québec (to M.F.), the Canadian Institutes of Health Research (PJT-169685 and PJT-175025 to M.F. and MOP-77686 to V.P.), the US National Institutes of Health (R01-DK-58096 to V.P.), and the CMDO Network (to M.F.). K.G. received scholarships from IRCM and the Natural Sciences and Engineering Research Council of Canada. J.L. received a fellowship from Diabetes Canada.

INCLUSION AND DIVERSITY

We support inclusive, diverse, and equitable conduct of research.

REFERENCES

1. Hudish LI, Reusch JE, and Sussel L (2019). Beta Cell dysfunction during progression of metabolic syndrome to type 2 diabetes. J. Clin. Invest 129, 4001–4008. 10.1172/JCI129188. [PubMed: 31424428]
2. Mehran AE, Templeman NM, Brigidi GS, Lim GE, Chu KY, Hu X, Botezelli JD, Asadi A, Hoffman BG, Kieffer TJ, et al. (2012). Hyper-insulinemia drives diet-induced obesity independently of brain insulin production. Cell Metabol. 16, 723–737. 10.1016/j.cmet.2012.10.019.
3. Mittendorfer B, Patterson BW, Smith GI, Yoshino M, and Klein S (2022). Beta Cell function and plasma insulin clearance in people with obesity and different glycemic status. J. Clin. Invest 132, e154068. 10.1172/JCI154068. [PubMed: 34905513]
4. Solis-Herrera C, Triplitt C, Cersosimo E, and DeFronzo RA (2000). Pathogenesis of Type 2 Diabetes Mellitus. In Endotext, Triplitt C, Cersosimo E, DeFronzo RA, Feingold KR, Anawalt B, Blackman MR, Boyce A, Chrousos G, and Corpas E, et al., eds.
5. Srour B, Fezeu LK, Kesse-Guyot E, Allès B, Debras C, Druesne-Pecollo N, Chazelas E, Deschasaux M, Hercberg S, Galan P, et al. (2020). Ultraprocessed food consumption and risk of type 2 diabetes among participants of the NutriNet-sante prospective cohort. JAMA Intern. Med 180, 283–291. 10.1001/jamainternmed.2019.5942. [PubMed: 31841598]

6. Kaidar-Person O, Person B, Szomstein S, and Rosenthal RJ (2008). Nutritional deficiencies in morbidly obese patients: a new form of malnutrition? Part A: vitamins. Obes. Surg 18, 870–876. 10.1007/s11695-007-9349-y. [PubMed: 18465178]
7. Hoffman DJ, Powell TL, Barrett ES, and Hardy DB (2021). Developmental origins of metabolic diseases. Physiol. Rev 101, 739–795. 10.1152/physrev.00002.2020. [PubMed: 33270534]
8. Via M (2012). The malnutrition of obesity: micronutrient deficiencies that promote diabetes. ISRN Endocrinol. 2012, 103472. 10.5402/2012/103472. [PubMed: 22462011]
9. Lacombe J, and Ferron M (2018). VKORC1L1, an enzyme mediating the effect of vitamin K in liver and extrahepatic tissues. Nutrients 10, E970. 10.3390/nu10080970.
10. Murshed M, Schinke T, McKee MD, and Karsenty G (2004). Extracellular matrix mineralization is regulated locally; different roles of two gla-containing proteins. J. Cell Biol 165, 625–630. [PubMed: 15184399]
11. Furie B, Bouchard BA, and Furie BC (1999). Vitamin K-dependent biosynthesis of gamma-carboxyglutamic acid. Blood 93, 1798–1808. [PubMed: 10068650]
12. Lee NK, Sowa H, Hinoi E, Ferron M, Ahn JD, Confavreux C, Dacquin R, Mee PJ, McKee MD, Jung DY, et al. (2007). Endocrine regulation of energy metabolism by the skeleton. Cell 130, 456–469. [PubMed: 17693256]
13. Ferron M, Lacombe J, Germain A, Oury F, and Karsenty G (2015). GGCX and VKORC1 inhibit osteocalcin endocrine functions. J. Cell Biol 208, 761–776. 10.1083/jcb.201409111. [PubMed: 25753038]
14. Pan Y, and Jackson RT (2009). Dietary phylloquinone intakes and metabolic syndrome in US young adults. J. Am. Coll. Nutr 28, 369–379. [PubMed: 20368375]
15. Beulens JWJ, van der A DL, Grobbee DE, Sluijs I, Spijkerman AMW, and van der Schouw YT (2010). Dietary phylloquinone and menaquinones intakes and risk of type 2 diabetes. Diabetes Care 33, 1699–1705. 10.2337/dc09-2302. [PubMed: 20424220]
16. Ibarrola-Jurado N, Salas-Salvadó J, Martínez-González MA, and Bulló M (2012). Dietary phylloquinone intake and risk of type 2 diabetes in elderly subjects at high risk of cardiovascular disease. Am. J. Clin. Nutr 96, 1113–1118. 10.3945/ajcn.111.033498. [PubMed: 23034962]
17. Ewang-Emukowhate M, Harrington DJ, Botha A, McGowan B, and Wierzbicki AS (2015). Vitamin K and other markers of micronutrient status in morbidly obese patients before bariatric surgery. Int. J. Clin. Pract 69, 638–642. 10.1111/ijcp.12594. [PubMed: 25496224]
18. Dihingia A, Ozah D, Ghosh S, Sarkar A, Baruah PK, Kalita J, Sil PC, and Manna P (2018). Vitamin K1 inversely correlates with glycemia and insulin resistance in patients with type 2 diabetes (T2D) and positively regulates SIRT1/AMPK pathway of glucose metabolism in liver of T2D mice and hepatocytes cultured in high glucose. J. Nutr. Biochem 52, 103–114. 10.1016/j.jnutbio.2017.09.022. [PubMed: 29175667]
19. Zwakenberg SR, Remmelzwaal S, Beulens JWJ, Booth SL, Burgess S, Dashti HS, Imamura F, Feskens EJM, van der Schouw YT, and Sluijs I (2019). Circulating phylloquinone concentrations and risk of type 2 diabetes: a mendelian randomization study. Diabetes 68, 220–225. 10.2337/db18-0543. [PubMed: 30352877]
20. Karamzad N, Faraji E, Adeli S, Carson-Chahhoud K, Azizi S, and Pourghassem Gargari B (2020). Effects of MK-7 supplementation on glycemic status, anthropometric indices and lipid profile in patients with type 2 diabetes: a randomized controlled trial. Diabetes Metab. Syndr. Obes 13, 2239–2249. 10.2147/DMSO.S253014. [PubMed: 32617013]
21. Rahimi Sakak F, Moslehi N, Niroomand M, and Mirmiran P (2021). Glycemic control improvement in individuals with type 2 diabetes with vitamin K2 supplementation: a randomized controlled trial. Eur. J. Nutr 60, 2495–2506. 10.1007/s00394-020-02419-6. [PubMed: 33159574]
22. Schmidt T, Samaras P, Frejno M, Gessulat S, Barnert M, Kienegger H, Krcmar H, Schlegl J, Ehrlich HC, Aiche S, et al. (2018). ProteomicsDB. Nucleic Acids Res. 46, D1271–D1281. 10.1093/nar/gkx1029. [PubMed: 29106664]
23. Tabula Muris Consortium; Overall coordination; Logistical coordination; Organ collection and processing; Library preparation and sequencing; Computational data analysis; Cell type annotation; Writing group; Supplemental text writing group; Principal investigators (2018).

Single-cell transcriptomics of 20 mouse organs creates a Tabula Muris. Nature 562, 367–372. 10.1038/s41586-018-0590-4. [PubMed: 30283141]

24. DiGruccio MR, Mawla AM, Donaldson CJ, Noguchi GM, Vaughan J, Cowing-Zitron C, van der Meulen T, and Huising MO (2016). Comprehensive alpha, beta and delta cell transcriptomes reveal that ghrelin selectively activates delta cells and promotes somatostatin release from pancreatic islets. Mol. Metabol 5, 449–458. 10.1016/j.molmet.2016.04.007.
25. Berkner KL, and Pudota BN (1998). Vitamin K-dependent carboxylation of the carboxylase. Proc. Natl. Acad. Sci. USA 95, 466–471. [PubMed: 9435215]
26. Lacombe J, Rishavy MA, Berkner KL, and Ferron M (2018). VKOR paralog VKORC1L1 supports vitamin K-dependent protein carboxylation in vivo. JCI Insight 3, e96501. 10.1172/jci.insight.96501. [PubMed: 29321368]
27. Haque JA, McDonald MG, Kulman JD, and Rettie AE (2014). A cellular system for quantitation of vitamin K cycle activity: structure-activity effects on vitamin K antagonism by warfarin metabolites. Blood 123, 582–589. 10.1182/blood-2013-05-505123. [PubMed: 24297869]
28. Shen G, Cui W, Zhang H, Zhou F, Huang W, Liu Q, Yang Y, Li S, Bowman GR, Sadler JE, et al. (2017). Warfarin traps human vitamin K epoxide reductase in an intermediate state during electron transfer. Nat. Struct. Mol. Biol 24, 69–76. 10.1038/nsmb.3333. [PubMed: 27918545]
29. Sharma RB, Landa-Galván HV, and Alonso LC (2021). Living dangerously: protective and harmful ER stress responses in pancreatic beta-cells. Diabetes 70, 2431–2443. 10.2337/dbi20-0033. [PubMed: 34711668]
30. Johnson JS, Kono T, Tong X, Yamamoto WR, Zarain-Herzberg A, Merrins MJ, Satin LS, Gilon P, and Evans-Molina C (2014). Pancreatic and duodenal homeobox protein 1 (Pdx-1) maintains endoplasmic reticulum calcium levels through transcriptional regulation of sarco-endoplasmic reticulum calcium ATPase 2b (SERCA2b) in the islet beta cell. J. Biol. Chem 289, 32798–32810. 10.1074/jbc.M114.575191. [PubMed: 25271154]
31. Wang IM, Zhang B, Yang X, Zhu J, Stepaniants S, Zhang C, Meng Q, Peters M, He Y, Ni C, et al. (2012). Systems analysis of eleven rodent disease models reveals an inflammasome signature and key drivers. Mol. Syst. Biol 8, 594. 10.1038/msb.2012.24. [PubMed: 22806142]
32. Motterle A, Gattesco S, Peyot ML, Esguerra JLS, Gomez-Ruiz A, Laybutt DR, Gilon P, Burdet F, Ibberson M, Eliasson L, et al. (2017). Identification of islet-enriched long non-coding RNAs contributing to beta-cell failure in type 2 diabetes. Mol. Metabol 6, 1407–1418. 10.1016/j.molmet.2017.08.005.
33. Lee H, Lee YS, Harenda Q, Pietrzak S, Oktay HZ, Schreiber S, Liao Y, Sonthalia S, Ciecko AE, Chen YG, et al. (2020). Beta cell dedifferentiation induced by IRE1alpha deletion prevents type 1 diabetes. Cell Metabol. 31, 822–836.e5. 10.1016/j.cmet.2020.03.002.
34. Ferdaoussi M, Dai X, Jensen MV, Wang R, Peterson BS, Huang C, Ilkayeva O, Smith N, Miller N, Hajmrle C, et al. (2015). Isocitrate-to-SENP1 signaling amplifies insulin secretion and rescues dysfunctional beta cells. J. Clin. Invest 125, 3847–3860. 10.1172/JCI82498. [PubMed: 26389676]
35. Brouwers B, de Faudeur G, Osipovich AB, Goyvaerts L, Lemaire K, Boesmans L, Cauwelier EJG, Granvik M, Pruniau VPEG, Van Lommel L, et al. (2014). Impaired islet function in commonly used trans genic mouse lines due to human growth hormone minigene expression. Cell Metabol. 20, 979–990. 10.1016/j.cmet.2014.11.004.
36. Oropeza D, Jouvet N, Budry L, Campbell JE, Bouyakdan K, Lacombe J, Perron G, Bergeron V, Neuman JC, Brar HK, et al. (2015). Phenotypic characterization of MIP-CreERT1Lphi mice with trans-gene-driven islet expression of human growth hormone. Diabetes 64, 3798–3807. 10.2337/db15-0272. [PubMed: 26153246]
37. Stamateris RE, Sharma RB, Hollern DA, and Alonso LC (2013). Adaptive beta-cell proliferation increases early in high-fat feeding in mice, concurrent with metabolic changes, with induction of islet cyclin D2 expression. Am. J. Physiol. Endocrinol. Metab 305, E149–E159. 10.1152/ajpendo.00040.2013. [PubMed: 23673159]
38. Sharma RB, O'Donnell AC, Stamateris RE, Ha B, McCloskey KM, Reynolds PR, Arvan P, and Alonso LC (2015). Insulin demand regulates beta cell number via the unfolded protein response. J. Clin. Invest 125, 3831–3846. 10.1172/JCI79264. [PubMed: 26389675]

39. Alquier T, and Poitout V (2018). Considerations and guidelines for mouse metabolic phenotyping in diabetes research. Diabetologia 61, 526–538. 10.1007/s00125-017-4495-9. [PubMed: 29143855]
40. Weldemariam MM, Woo J, and Zhang Q (2022). Pancreatic INS-1 beta-cell response to thapsigargin and rotenone: a comparative proteomics analysis uncovers key pathways of beta-cell dysfunction. Chem. Res. Toxicol 35, 1080–1094. 10.1021/acs.chemrestox.2c00058. [PubMed: 35544339]
41. Feriotto G, Finotti A, Volpe P, Treves S, Ferrari S, Angelelli C, Zorzato F, and Gambari R (2005). Myocyte enhancer factor 2 activates promoter sequences of the human AbetaH-J-J locus, encoding aspartyl-beta-hydroxylase, junctin, and junctate. Mol. Cell Biol 25, 3261–3275. 10.1128/MCB.25.8.3261-3275.2005. [PubMed: 15798210]
42. Dinchuk JE, Henderson NL, Burn TC, Huber R, Ho SP, Link J, O'Neil KT, Focht RJ, Scully MS, Hollis JM, et al. (2000). Aspartyl beta -hydroxylase (Asph) and an evolutionarily conserved isoform of Asph missing the catalytic domain share exons with junctin. J. Biol. Chem 275, 39543–39554. 10.1074/jbc.M006753200. [PubMed: 10956665]
43. Feriotto G, Finotti A, Breveglieri G, Treves S, Zorzato F, and Gambari R (2006). Multiple levels of control of the expression of the human A beta H-J-J locus encoding aspartyl-beta-hydroxylase, junctin, and junctate. Ann. N. Y. Acad. Sci 1091, 184–190. 10.1196/annals.1378.065. [PubMed: 17341613]
44. Srikanth S, Jew M, Kim KD, Yee MK, Abramson J, and Gwack Y (2012). Junctate is a Ca2+-sensing structural component of Orai1 and stromal interaction molecule 1 (STIM1). Proc. Natl. Acad. Sci. USA 109, 8682–8687. 10.1073/pnas.1200667109. [PubMed: 22586105]
45. Lunz V, Romanin C, and Frischauf I (2019). STIM1 activation of Orai1. Cell Calcium 77, 29–38. 10.1016/j.ceca.2018.11.009. [PubMed: 30530091]
46. Samtleben S, Wachter B, and Blum R (2015). Store-operated calcium entry compensates fast ER calcium loss in resting hippocampal neurons. Cell Calcium 58, 147–159. 10.1016/j.ceca.2015.04.002. [PubMed: 25957620]
47. Palty R, Raveh A, Kaminsky I, Meller R, and Reuveny E (2012). SARAF inactivates the store operated calcium entry machinery to prevent excess calcium refilling. Cell 149, 425–438. 10.1016/j.cell.2012.01.055. [PubMed: 22464749]
48. Sabourin J, Le Gal L, Saurwein L, Haefliger JA, Raddatz E, and Allagnat F (2015). Store-operated Ca2+ entry mediated by Orai1 and TRPC1 participates to insulin secretion in rat beta-cells. J. Biol. Chem 290, 30530–30539. 10.1074/jbc.M115.682583. [PubMed: 26494622]
49. Kono T, Tong X, Taleb S, Bone RN, Iida H, Lee CC, Sohn P, Gilon P, Roe MW, and Evans-Molina C (2018). Impaired store-operated calcium entry and STIM1 loss lead to reduced insulin secretion and increased endoplasmic reticulum stress in the diabetic beta-cell. Diabetes 67, 2293–2304. 10.2337/db17-1351. [PubMed: 30131394]
50. Greotti E, Wong A, Pozzan T, Pendin D, and Pizzo P (2016). Characterization of the ER-targeted low affinity Ca(2+) probe D4ER. Sensors 16, 1419. 10.3390/s16091419. [PubMed: 27598166]
51. Yong J, Parekh VS, Reilly SM, Nayak J, Chen Z, Lebeaupin C, Jang I, Zhang J, Prakash TP, Sun H, et al. (2021). Chop/Ddit3 depletion in beta cells alleviates ER stress and corrects hepatic steatosis in mice. Sci. Transl. Med 13, eaba9796. 10.1126/scitranslmed.aba9796. [PubMed: 34321322]
52. Roe MW, Philipson LH, Frangakis CJ, Kuznetsov A, Mertz RJ, Lancaster ME, Spencer B, Worley JF 3rd, and Dukes ID (1994). Defective glucose-dependent endoplasmic reticulum Ca2+ sequestration in diabetic mouse islets of Langerhans. J. Biol. Chem 269, 18279–18282. [PubMed: 8034570]
53. Liu X, Feng S, Chen Z, Zhou Y, Yin K, Xue Z, and Zhu W (2022). Is the risk of diabetes lower in patients with atrial fibrillation treated with direct oral anticoagulant compared to warfarin? Front. Cardiovasc. Med 9, 874795. 10.3389/fcvm.2022.874795. [PubMed: 35665262]
54. Cheung CL, Sing CW, Lau WCY, Li GHY, Lip GYH, Tan KCB, Cheung BMY, Chan EWY, and Wong ICK (2021). Treatment with direct oral anticoagulants or warfarin and the risk for incident diabetes among patients with atrial fibrillation: a population-based cohort study. Cardiovasc. Diabetol 20, 71. 10.1186/s12933-021-01263-0. [PubMed: 33766030]

55. Schulte A, and Blum R (2022). Shaped by leaky ER: homeostatic Ca(2+) fluxes. Front. Physiol 13, 972104. 10.3389/fphys.2022.972104. [PubMed: 36160838]
56. Mamenko M, Dhande I, Tomilin V, Zaika O, Boukelmoune N, Zhu Y, Gonzalez-Garay ML, Pochynyuk O, and Doris PA (2016). Defective store-operated calcium entry causes partial nephrogenic diabetes insipidus. J. Am. Soc. Nephrol 27, 2035–2048. 10.1681/ASN.2014121200. [PubMed: 26574044]
57. Park CY, Hoover PJ, Mullins FM, Bachhawat P, Covington ED, Raunser S, Walz T, Garcia KC, Dolmetsch RE, and Lewis RS (2009). STIM1 clusters and activates CRAC channels via direct binding of a cytosolic domain to Orai1. Cell 136, 876–890. 10.1016/j.cell.2009.02.014. [PubMed: 19249086]
58. Treves S, Franzini-Armstrong C, Moccagatta L, Arnoult C, Grasso C, Schrum A, Ducreux S, Zhu MX, Mikoshiba K, Girard T, et al. (2004). Junctate is a key element in calcium entry induced by activation of InsP3 receptors and/or calcium store depletion. J. Cell Biol 166, 537–548. 10.1083/jcb.200404079. [PubMed: 15302852]
59. Kwon SJ, and Kim DH (2009). Characterization of junctate-SERCA2a interaction in murine cardiomyocyte. Biochem. Biophys. Res. Commun 390, 1389–1394. 10.1016/j.bbrc.2009.10.165. [PubMed: 19896466]
60. Zhang IX, Ren J, Vadrevu S, Raghavan M, and Satin LS (2020). ER stress increases store-operated Ca(2+) entry (SOCE) and augments basal insulin secretion in pancreatic beta cells. J. Biol. Chem 295, 5685–5700. 10.1074/jbc.RA120.012721. [PubMed: 32179650]
61. Sabatini PV, Speckmann T, and Lynn FC (2019). Friend and foe: beta-cell Ca(2+) signaling and the development of diabetes. Mol. Metabol 21, 1–12. 10.1016/j.molmet.2018.12.007.
62. Liang K, Du W, Lu J, Li F, Yang L, Xue Y, Hille B, and Chen L (2014). Alterations of the Ca(2)(+) signaling pathway in pancreatic beta-cells isolated from db/db mice. Protein Cell 5, 783–794. 10.1007/s13238-014-0075-7. [PubMed: 25053525]
63. Stenflo J, Fernlund P, Egan W, and Roepstorff P (1974). Vitamin K dependent modifications of glutamic acid residues in prothrombin. Proc. Natl. Acad. Sci. USA 71, 2730–2733. [PubMed: 4528109]
64. Perez-Riverol Y, Bai J, Bandla C, García-Seisdedos D, Hewapathirana S, Kamatchinathan S, Kundu DJ, Prakash A, Frericks-Zipper A, Eisenacher M, et al. (2022). The PRIDE database resources in 2022: a hub for mass spectrometry-based proteomics evidences. Nucleic Acids Res. 50, D543–D552. 10.1093/nar/gkab1038. [PubMed: 34723319]
65. Hingorani SR, Petricoin EF, Maitra A, Rajapakse V, King C, Jacobetz MA, Ross S, Conrads TP, Veenstra TD, Hitt BA, et al. (2003). Preinvasive and invasive ductal pancreatic cancer and its early detection in the mouse. Cancer Cell 4, 437–450. [PubMed: 14706336]
66. Thorens B, Tarussio D, Maestro MA, Rovira M, Heikkilä E, and Ferrer J (2015). Ins1(Cre) knock-in mice for beta cell-specific gene recombination. Diabetologia 58, 558–565. 10.1007/s00125-014-3468-5. [PubMed: 25500700]
67. Lyon J, Manning Fox JE, Spigelman AF, Kim R, Smith N, O'Gorman D, Kin T, Shapiro AMJ, Rajotte RV, and MacDonald PE (2016). Research-focused isolation of human islets from donors with and without diabetes at the Alberta diabetes Institute IsletCore. Endocrinology 157, 560–569. 10.1210/en.2015-1562. [PubMed: 26653569]
68. Lyon J, Spigelman AF, MacDonald PE, and Manning Fox JE (2019). ADI isletcore protocols for the isolation, assessment and cryopreservation of human pancreatic islets of langerhans for research purposes V.1. Protocol. 10.17504/protocols.io.x3mfqk6.
69. Ronnebaum SM, Jensen MV, Hohmeier HE, Burgess SC, Zhou YP, Qian S, MacNeil D, Howard A, Thornberry N, Ilkayeva O, et al. (2008). Silencing of cytosolic or mitochondrial isoforms of malic enzyme has no effect on glucose-stimulated insulin secretion from rodent islets. J. Biol. Chem 283, 28909–28917. 10.1074/jbc.M804665200. [PubMed: 18755687]
70. Hagman DK, Latour MG, Chakrabarti SK, Fontes G, Amyot J, Tremblay C, Semache M, Lausier JA, Roskens V, Mirmira RG, et al. (2008). Cyclical and alternating infusions of glucose and intralipid in rats inhibit insulin gene expression and Pdx-1 binding in islets. Diabetes 57, 424–431. 10.2337/db07-1285. [PubMed: 17991758]

71. Moullé VS, Vivot K, Tremblay C, Zarrouki B, Ghislain J, and Poitout V (2017). Glucose and fatty acids synergistically and reversibly promote beta cell proliferation in rats. Diabetologia 60, 879–888. 10.1007/s00125-016-4197-8. [PubMed: 28078385]
72. Ghosh S, Kraus K, Biswas A, Müller J, Buhl AL, Forin F, Singer H, Höning K, Hornung V, Watzka M, et al. (2021). GGCX mutations show different responses to vitamin K thereby determining the severity of the hemorrhagic phenotype in VKCFD1 patients. J. Thromb. Haemostasis 19, 1412–1424. 10.1111/jth.15238. [PubMed: 33590680]
73. Tie JK, Jin DY, Straight DL, and Stafford DW (2011). Functional study of the vitamin K cycle in mammalian cells. Blood 117, 2967–2974. 10.1182/blood-2010-08-304303. [PubMed: 21239697]
74. Lacombe J, Al Rifai O, Loter L, Moran T, Turcotte AF, Grenier-Larouche T, Tchernof A, Biertho L, Carpentier AC, Prud'homme D, et al. (2020). Measurement of bioactive osteocalcin in humans using a novel immunoassay reveals association with glucose metabolism and beta-cell function. Am. J. Physiol. Endocrinol. Metab 318, E381–E391. 10.1152/ajpendo.00321.2019. [PubMed: 31935114]
75. Al Rifai O, Chow J, Lacombe J, Julien C, Faubert D, Susan-Resiga D, Essalmani R, Creemers JW, Seidah NG, and Ferron M (2017). Proprotein convertase furin regulates osteocalcin and bone endocrine function. J. Clin. Invest 127, 4104–4117. 10.1172/JCI93437. [PubMed: 28972540]
76. Chomczynski P, and Sacchi N (2006). The single-step method of RNA isolation by acid guanidinium thiocyanate-phenol-chloroform extraction: twenty-something years on. Nat. Protoc 1, 581–585. 10.1038/nprot.2006.83. [PubMed: 17406285]
77. Oh-Hora M, Yamashita M, Hogan PG, Sharma S, Lamperti E, Chung W, Prakriya M, Feske S, and Rao A (2008). Dual functions for the endoplasmic reticulum calcium sensors STIM1 and STIM2 in T cell activation and tolerance. Nat. Immunol 9, 432–443. 10.1038/ni1574. [PubMed: 18327260]
78. Schindelin J, Arganda-Carreras I, Frise E, Kaynig V, Longair M, Pietzsch T, Preibisch S, Rueden C, Saalfeld S, Schmid B, et al. (2012). Fiji: an open-source platform for biological-image analysis. Nat. Methods 9, 676–682. 10.1038/nmeth.2019. [PubMed: 22743772]
79. Ferron M, Boudiffa M, Arsenault M, Rached M, Pata M, Giroux S, Elfassihi L, Kisseleva M, Majerus PW, Rousseau F, and Vacher J (2011). Inositol polyphosphate 4-phosphatase B as a regulator of bone mass in mice and humans. Cell Metabol. 14, 466–477.
80. Picard M, Petrie RJ, Antoine-Bertrand J, Saint-Cyr-Proulx E, Villemure JF, and Lamarche-Vane N (2009). Spatial and temporal activation of the small GTPases RhoA and Rac1 by the netrin-1 receptor UNC5a during neurite outgrowth. Cell. Signal 21, 1961–1973. 10.1016/j.cellsig.2009.09.004. [PubMed: 19755150]
81. Xia Z, and Liu Y (2001). Reliable and global measurement of fluorescence resonance energy transfer using fluorescence microscopes. Biophys. J 81, 2395–2402. 10.1016/S0006-3495(01)75886-9. [PubMed: 11566809]
82. Szklarczyk D, Gable AL, Nastou KC, Lyon D, Kirsch R, Pyysalo S, Doncheva NT, Legeay M, Fang T, Bork P, et al. (2021). The STRING database in 2021: customizable protein-protein networks, and functional characterization of user-uploaded gene/measurement sets. Nucleic Acids Res. 49, D605–D612. 10.1093/nar/gkaa1074. [PubMed: 33237311]
83. Bardou P, Mariette J, Escudié F, Djemiel C, and Klopp C (2014). jvenn: an interactive Venn diagram viewer. BMC Bioinf. 15, 293. 10.1186/1471-2105-15-293.

Highlights

- Vitamin K-dependent carboxylation regulates glucose-stimulated insulin secretion
- ERGP is a γ-carboxylated protein controlling store-operated calcium entry
- ERGP γ-carboxylation reduces STIM1 and Orai1 puncta formation
- Decarboxylated ERGP causes calcium overfilling in β cells and hyperinsulinemia

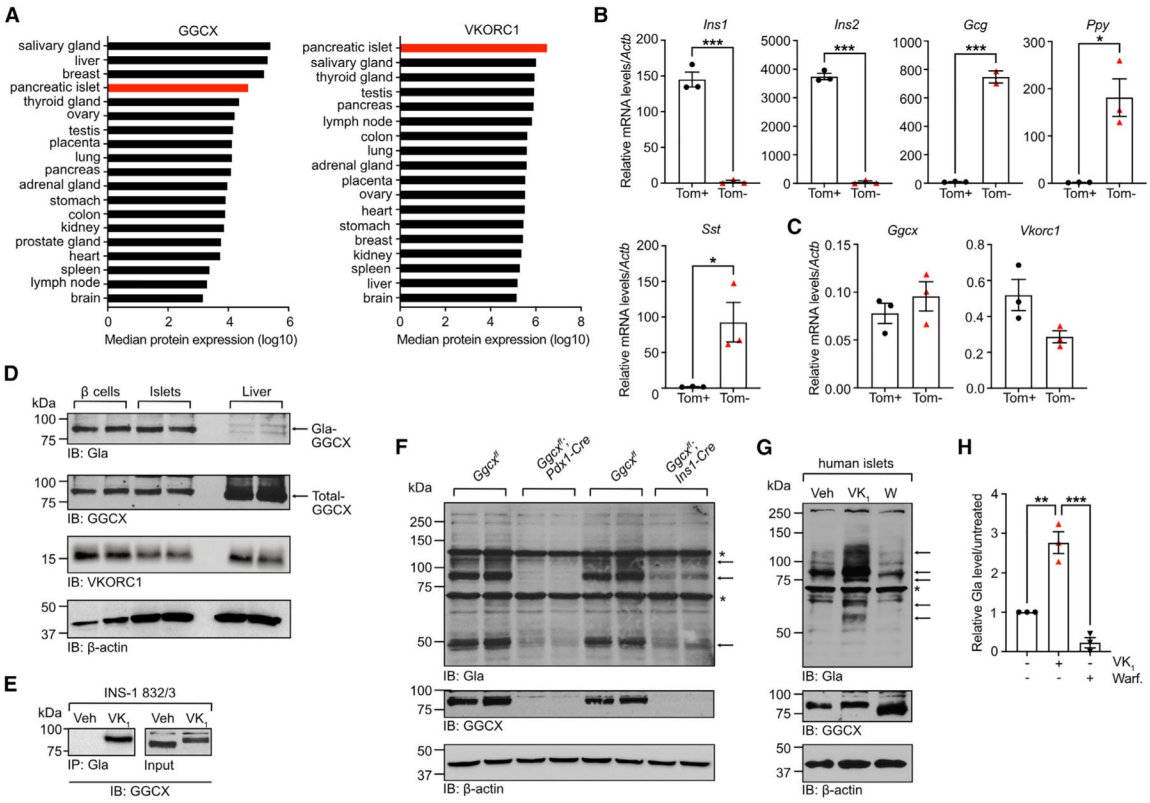

Figure 1. VK-dependent carboxylation machinery is active in islets and β cells

(A) GGCX and VKORC1 protein in human tissues expressed as normalized intensity-based absolute quantification (iBAQ; www.proteomicsdb.org).

(B and C) Gene expression analysis by qPCR on sorted β cells (Tom^+) and on other endocrine islet cells (Tom^-) (n = 3).

(D) Protein expression in β cells, islets, and livers from *Ins1*$^{Cre/+}$; *Rosa26*$^{CAG\text{-}lox\text{-}stop\text{-}lox\text{-}tdTomato}$ mice by western blot.

(E) γ-Carboxylation in INS-1 832/3 cells cultured with vitamin K_1 (VK_1; 22μM) or vehicle, analyzed by anti-Gla IP and western blot.

(F) Islets from *Ggcx*^{ff}*; Pdx1-Cre* and *Ggcx*^{ff}*; Ins1-Cre* mice and their respective *Ggcx*^{ff} littermates, analyzed by western blot.

(G and H) Human islets from non-diabetic cadaveric donors cultured in the presence of VK_1 (22 μM), warfarin (50 μM), or vehicle, analyzed by western blot.

(G) Representative western blot experiment with islets from donor R266.

(H) γ-Carboxylation quantified using arbitrary densitometry units of Gla signals over β-actin signals. Data from VK_1− and warfarin-treated samples were normalized over vehicle treatment (n = 3).

Results represent the mean ± SEM. Unpaired, 2-tailed Student's t test was used in (B) and (C). Ordinary one-way ANOVA with Bonferroni's post tests was used in (H). ***$p < 0.001$, **$p < 0.01$, *$p < 0.05$. See also Figure S1 and Table S1.

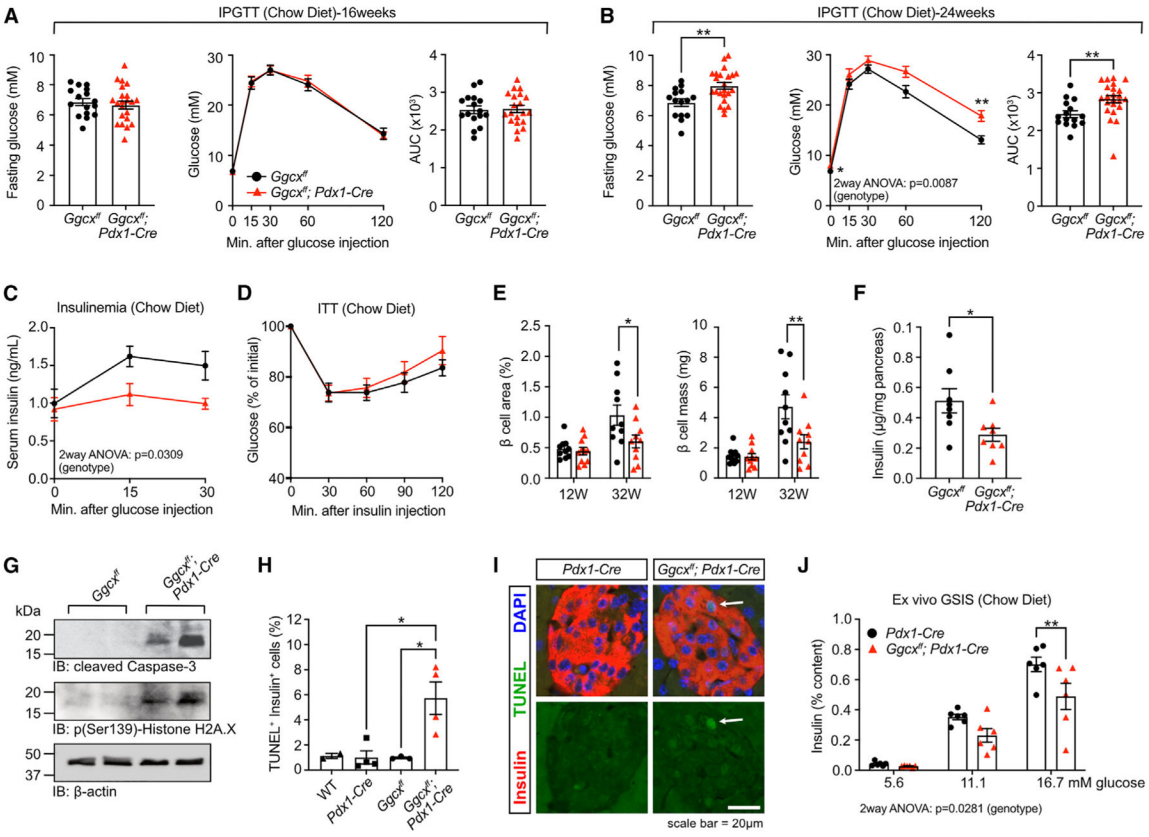

Figure 2. GGCX is necessary for maintenance of an adequate β cell mass in adult mice

(A and B) Intraperitoneal glucose tolerance test (IPGTT) performed on (A) 16-week-old (n = 16–21) and (B) 24-week-old (n = 15–23) *Ggcx^{ff}; Pdx1-Cre* and *Ggcx^{ff}* male mice.

(C) Insulinemic response to glucose measured in 24-week-old male mice (n = 10).

(D) Insulin tolerance test (ITT) in 24-week-old male mice (n = 9–10).

(E) Histomorphometric analysis on pancreas sections following insulin staining and hematoxylin counterstaining on 12- and 32-week-old mice (n = 10–11).

(F) Pancreas insulin content from 24- to 28-week-old *Ggcx^{ff}; Pdx1-Cre* and *Ggcx^{ff}* male mice (n = 8).

(G) Western blot analysis on islets from *Ggcx^{ff}; Pdx1-Cre* mice.

(H) TUNEL and insulin co-staining on pancreas sections from 32-week-old mice (n = 2–4).

(I) Representative picture showing TUNEL^{+} insulin^{+} β cells in pancreas sections from *Ggcx^{ff}; Pdx1-Cre* mice (indicated by the white arrow).

(J) Static *ex vivo* glucose-stimulated insulin secretion (GSIS) test on isolated islets from *Pdx1-Cre* and *Ggcx^{ff}; Pdx1-Cre* mice (n = 6).

Results represent the mean ± SEM. Unpaired, 2-tailed Student's t test was used in (A) and (B) for fasting glucose and area under the curve (AUC) and in (F). Two-way ANOVA with Bonferroni's post tests was used in (A) and (B) for IPGTTs and in (C)–(E) and (J). Ordinary one-way ANOVA with Bonferroni's post tests was used in (H). ***p < 0.001, **p < 0.01, *p < 0.05. See also Figures S2 and S3 and Tables S2 and S3.

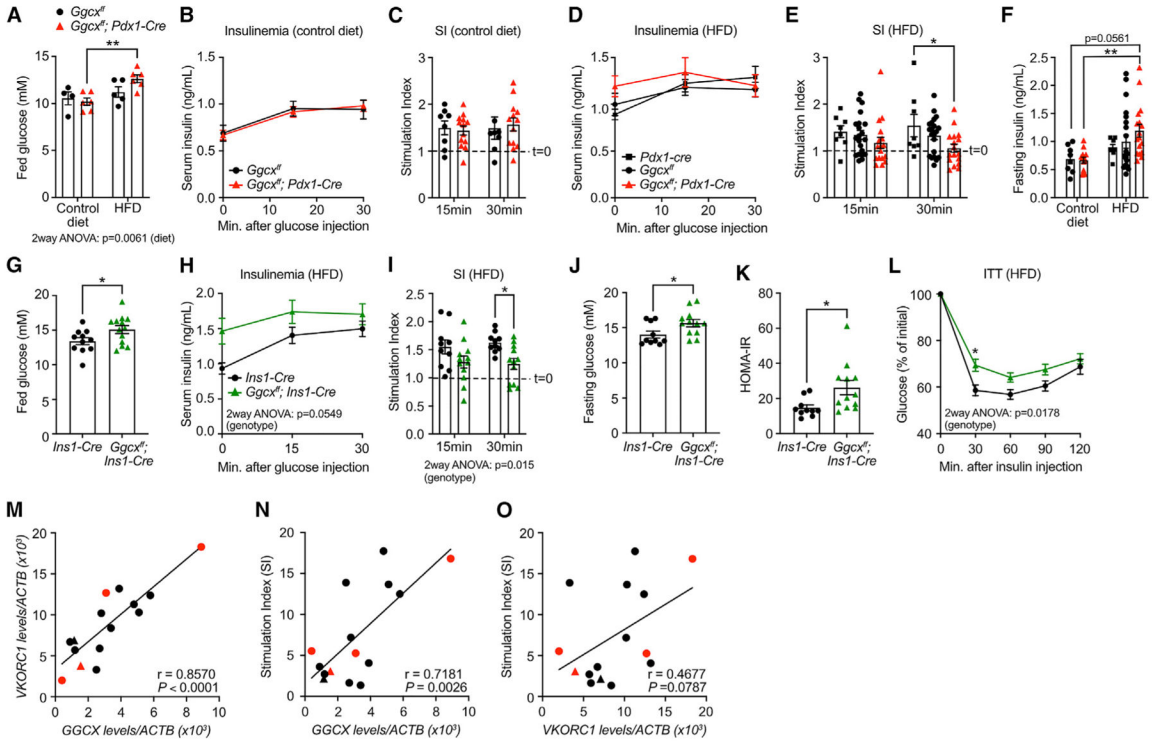

Figure 3. Pancreas or β cell specific deletion of *Ggcx* compromises insulin secretion in response to an HFD

(A–L) Ten-week-old male mice of different genotypes were fed with an HFD (60%) or a control low-fat diet (10%) for 7 days, and metabolic analysis was performed.

(A) Fed blood glucose level for *Ggcx^{ff}; Pdx1-Cre* and *Ggcx^{ff}* male mice (n = 4–6).

(B and C) For control low-fat-diet-fed *Ggcx^{ff}; Pdx1-Cre* and *Ggcx^{ff}* mice, the insulinemic response is represented in (B) absolute value and (C) as SI (blood insulin concentration at 15 or 30 min over T0). The dashed line represents an SI of 1 at fasting.

(D–F) For HFD-fed *Ggcx^{ff}; Pdx1-Cre*, *Ggcx^{ff}* and *Pdx1-Cre* mice, the insulinemic response to glucose is represented in (D) absolute value or (E) as SI, and (F) fasting insulin levels are shown (n = 8–21).

(G–L) Metabolic analysis of *Ggcx^{ff}; Ins1-Cre* and *Ins1-Cre* mice following 7 days of HFD feeding: (G) fed blood glucose, (H and I) insulinemic response to glucose, (J) fasting blood glucose, (K) HOMA-IR, and (L) ITT (n = 10–13).

(M–O) Correlation in 15 human islet donor samples between (M) *Ggcx* and *Vkorc1* gene expression levels and between (N) *Ggcx* or (O) *Vkorc1* and each sample's SI (insulin secretion at 10 mM over 1 mM glucose).

Black circles represent non-diabetic male donors, red circles diabetic male donors, black triangles non-diabetic female donors, and red triangles diabetic female donors. Results represent the mean ± SEM. Two-way ANOVA with Bonferroni's post tests was used in (A)–(E), (H)–(I), and (L). Ordinary one-way ANOVA with Bonferroni's post tests was used in (F). Unpaired, 2-tailed Student's t test was used in (G), (J), and (K). Pearson's correlation was used in (M)–(O). **p < 0.01, *p < 0.05. See also Figure S4.

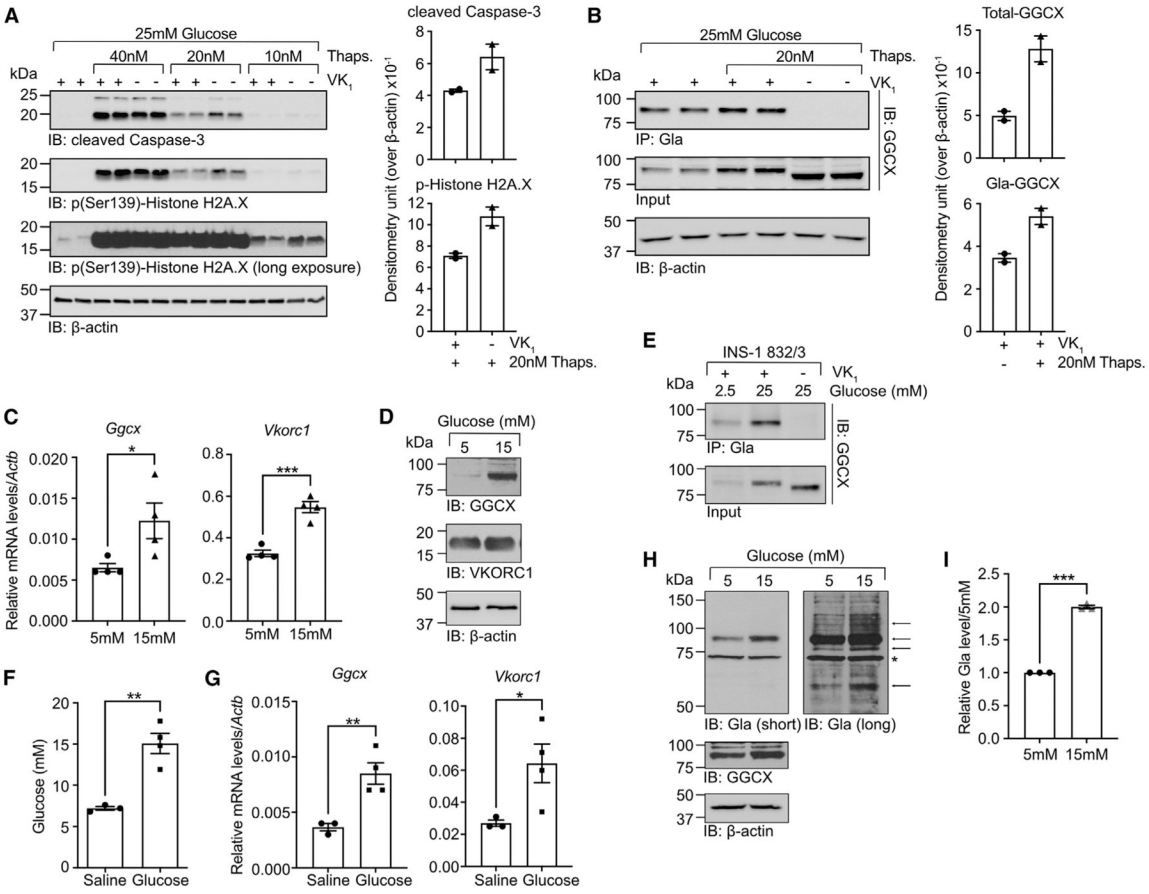

Figure 4. γ-Carboxylation protects β cells from ER stress-induced cell death and is regulated by glucose

(A and B) INS-1 832/3 cells were cultured with VK_1 (22 μM) or vehicle for 48 h before being cultured for 24 h in medium containing 25 mM glucose and thapsigargin.

(A) Cellular fitness was analyzed by western blot using cleaved caspase-3 and p(Ser139)-histone H2A.X antibodies. Quantification was performed using arbitrary densitometry units of cleaved caspase-3 and p(Ser139)-histone H2A.X signals obtained in samples treated with 20 nM thapsigargin over b-actin signals.

(B) GGCX γ-carboxylation assessed by anti-Gla IP followed by Western blot using anti-GGCX antibodies. Quantification was performed using arbitrary densitometry units of GGCX and Gla-GGCX signals over b-actin signals.

(C and D) Islets from C57BL/6J mice were cultured in medium containing either 5 or 15 mM glucose, and expression was analyzed by (C) qPCR (n = 3–4) and (D) western blot.

(E) INS-1 832/3 cells were cultured in medium containing 2.5 or 25 mM glucose in the presence of VK_1 (22 μM) or vehicle, and GGCX γ-carboxylation was assessed by anti-Gla IP followed by western blot.

(F and G) Two-months old Wistar rats were infused during 3 days with saline or glucose.

(F) Average blood glucose level for each mouse.

(G) Gene expression analyzed by qPCR (n = 3–4).

(H and I) Human islets from non-diabetic cadaveric donors were cultured in the presence of VK_1 (22 μM) in medium containing either 5 or 15 mM glucose for 3 days.

(H) Representative western blot experiment with islets from donor R288.

(I) γ-Carboxylation was quantified using arbitrary densitometry units of Gla signals over b-actin signals.

Data from 15 mM glucose-treated samples were normalized over 5 mM glucose treatment (n = 3). Results represent the mean ± SEM. Unpaired, 2-tailed Student's t test was used in (C), (F), (G), and (I). ***$p < 0.001$, **$p < 0.01$, *$p < 0.05$. See also Figure S5 and Table S1.

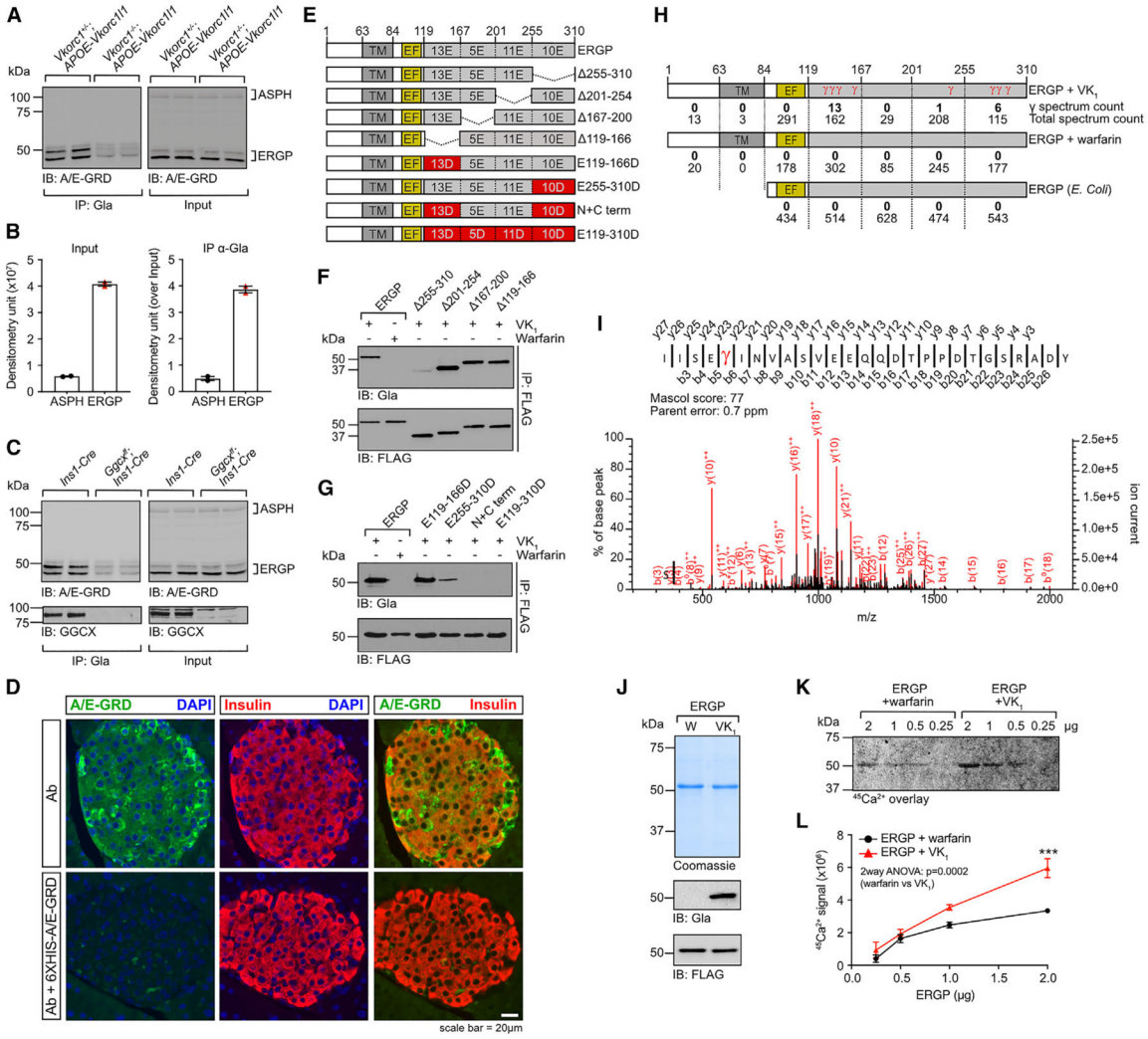

Figure 5. ERGP is a γ-carboxylated protein expressed in β cells

(A) ASPH and ERGP γ-carboxylation in *Vkorc1*$^{+/-}$*; APOE-Vkorc1l1*, and *Vkorc1*$^{-/-}$*; APOE-Vkorc1l1* mouse islets, assessed by IP with anti-Gla antibody followed by western blot.

(B) Expression and γ-carboxylation, quantified using arbitrary densitometry units of ASPH and ERGP signals.

(C) ASPH, ERGP, and GGCX γ-carboxylation in *Ggcx*^{ff}*; Ins1-Cre* and *Ins1-Cre* mouse islets, assessed by IP with anti-Gla antibody followed by western blot.

(D) Immunofluorescence on pancreas sections from WT mice using anti-A/E-GRD and anti-insulin antibodies. Competition with recombinant 6×His-A/E-GRD protein was used to demonstrate specificity of the antibody.

(E) Schematic of the constructs used in (F) and (G).

(F and G) HEK293 cells transfected with the indicated constructs were cultured with VK_1 (22 μM) or warfarin (50 μM) as specified. FLAG-tagged proteins were immunoprecipitated, followed by western blotting with anti-Gla or anti-FLAG antibodies.

(H) Schematic of ERGP, indicating the total number of γ-carboxylated spectrum counts detected by L-MS/MS.
(I) Representative LC-MS/MS spectrum showing a γ-carboxylated residue in the peptide ranging from residues 289–316 in purified ERGP-3×FLAG expressed in HEK293 cells grown in the presence of VK_1.
(J) ERGP-3×FLAG purified from HEK293 cells cultured with VK_1 (γ-carboxylated) or warfarin (uncarboxylated) was stained with Coomassie, and γ-carboxylation was monitored by western blot using anti-Gla antibodies.
(K) Membrane-immobilized γ-carboxylated and non-carboxylated ERGP-3×FLAG was incubated with $^{45}Ca^{2+}$, and radioactivity was detected using a storage PhosphorImager screen.
(L) Ca^{2+} binding quantified using arbitrary densitometry units (n = 3).
Results represent the mean ± SEM. Two-way ANOVA with Bonferroni's post tests was used in (L). ***$p < 0.001$. See also Figure S6 and Tables S4, S5, and S6.

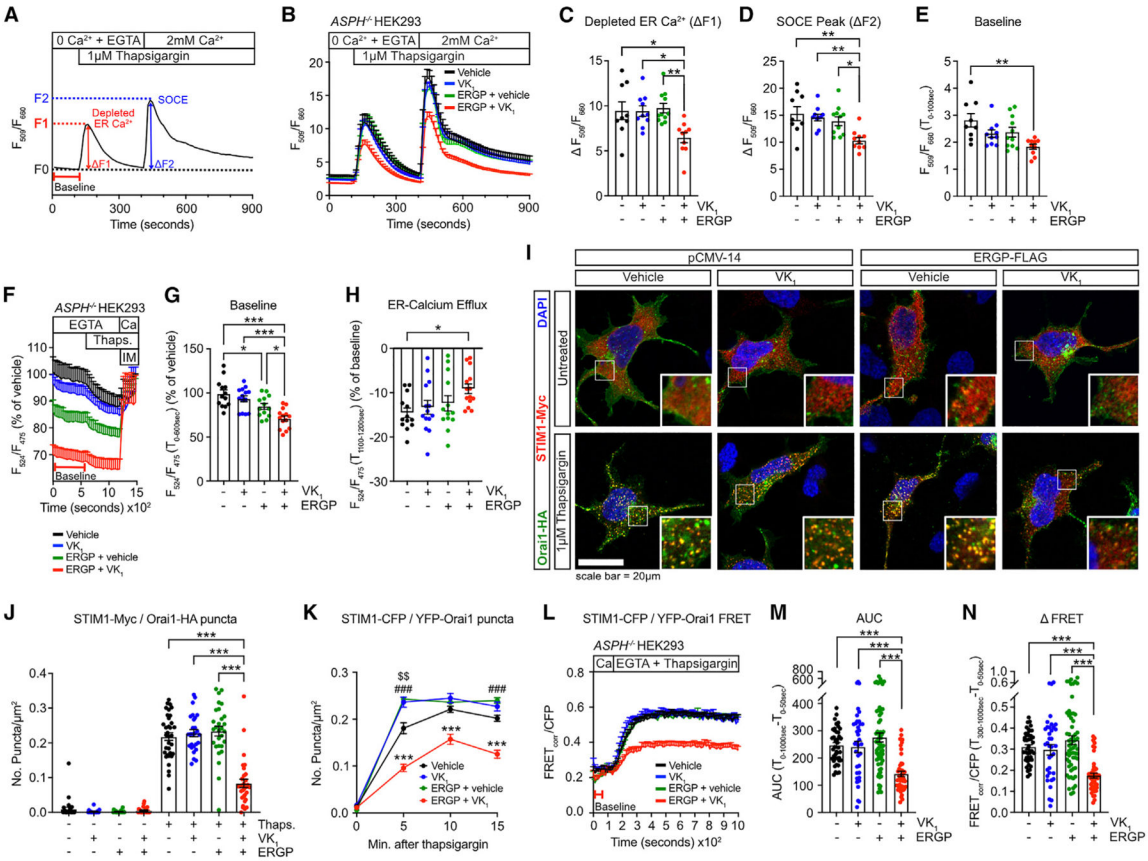

Figure 6. ERGP γ-carboxylation regulates Ca^{2+} flux by modulating STIM1/Orai1 interaction

(A) Representation of the strategy used to measure and quantify store-operated Ca^{2+} entry (SOCE) by live-cell imaging.

(B) Ca^{2+} imaging traces are represented as the ratio between Fluo-4 and Fura Red emission intensity (F_{509}/F_{660}) for each condition (n = 9–11 experimental replicates per condition).

(C and D) Quantification of (C) depleted ER Ca^{2+}; (D) SOCE peak are represented as ΔF1 and ΔF2 respectively, as described in (A).

(E) Baseline cytosolic Ca^{2+} defined as the average F_{509}/F_{660} ratio during the first 100 s of recording.

(F–H) Measurements of ER Ca^{2+} levels in *ASPH*$^{-/-}$ HEK293 cells transfected with the D4ER ratiometric Ca^{2+} probe (n = 11–14 experimental replicates per condition).

(F) Representative experiment showing D4ER Ca^{2+} imaging traces expressed as a ratio between the citrine FRET emission and CFP emission (F_{524}/F_{475}) for each condition. Data are normalized to the mean of the first recorded 100 s of the vehicle condition and are represented as percentage of vehicle.

(G) Baseline ER Ca^{2+} defined as the average F_{524}/F_{475} ratio during the 600 s of recording before thapsigargin addition. Data are represented as percentage of vehicle.

(H) ER Ca^{2+} efflux following thapsigargin, corresponding to the average F_{524}/F_{475} ratio recorded during the last 100 s of the thapsigargin treatment, expressed as a percentage of the average of the F_{524}/F_{475} ratio recorded at baseline.

(I) Representative confocal immunofluorescence images of *ASPH*$^{-/-}$HEK293 cells transfected as in (B) and treated with 1 μM thapsigargin or vehicle for 15 min.
(J) Quantification of co-localized STIM1-myc and Orai1-HA puncta from the experiment in (I) (n = 27–34 cells per condition).
(K) Quantification of CFP and YFP co-expressing puncta in *ASPH*$^{-/-}$HEK293 cells transfected with STIM1-CFP and YFP-Orai1 plasmids (n = 37–61 cells per condition).
(L–N) STIM1-CFP and YFP-Orai1 SOCE complex formation measured by FRET. STIM1-CFP/YFP-Orai1 complex formation was triggered by addition of 3 mM EGTA and 1 μM thapsigargin 120 s after starting recording (n = 37–61 cells per condition).
(L) FRET signal traces averaged from individual cells, represented as corrected FRET intensity over CFP intensity ($FRET_{corr}$/CFP).
(M) Area under the curve (AUC) of $FRET_{corr}$/CFP traces in (L) from baseline to thapsigargin FRET signal from individual cells for each condition.
(N) Average change in $FRET_{corr}$/CFP from baseline (average T0–50s) to peak after thapsigargin and Ca^{2+} depletion (average T300–1000s).
Results represent the mean ± SEM. Ordinary one-way ANOVA with Bonferroni's post tests was used in (C)–(E), (G), (H), (J), (M), and (N). Two-way ANOVA with Bonferroni's post tests was used in (K). ***p < 0.001, **p < 0.01, *p < 0.05. In (K), * represents comparison between ERGP+VK_1 and every other condition, # represents comparison between vehicle and ERGP, and $ represents comparison between vehicle and VK_1. See also Figure S7.

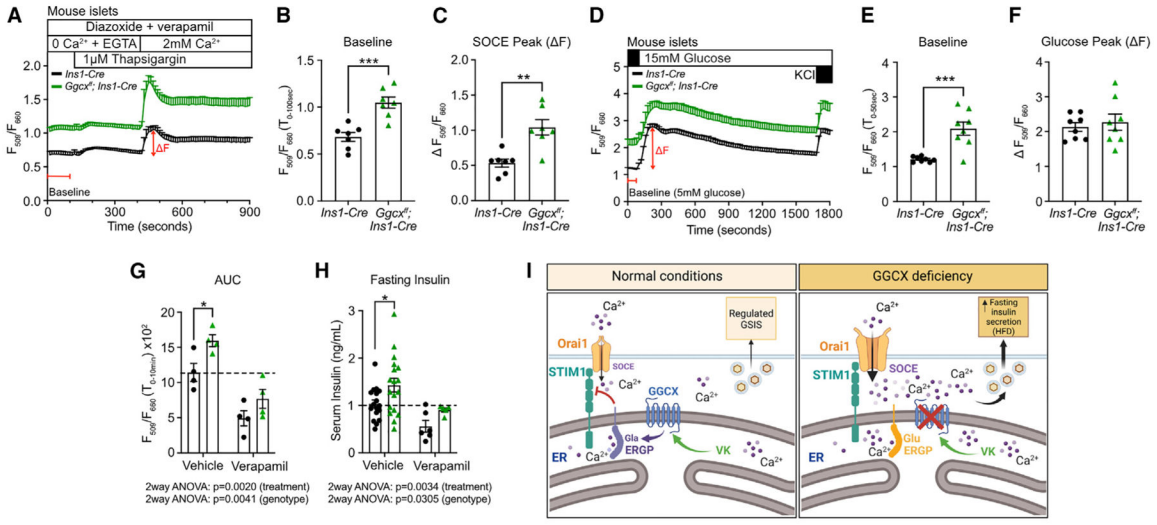

Figure 7. Increased SOCE and basal cytosolic Ca^{2+} in *Ggcx*-deficient β cells cause impaired fasting hyperinsulinemia

(A) SOCE measured by live-cell Ca^{2+} imaging in semi-dispersed islets from *Ggcx^{ff}; Ins1-Cre* and *Ins1-Cre* mice at 5 mM glucose (n = 7 experimental replicates per condition).

(B and C) Quantification of (B) baseline cytosolic Ca^{2+} level, defined as the average F_{509}/F_{660} ratio during the first 100 s of recording, and (C) SOCE peak (ΔF).

(D) Cytosolic Ca^{2+} level measured at 5 and 15 mM glucose (n = 8 experimental replicates per condition).

(E) Baseline cytosolic Ca^{2+} level during the first 50 s of recording and (F) glucose-stimulated Ca^{2+} peak (ΔF) quantification.

(G) Quantification of Ca^{2+} imaging experiments of semi-dispersed islets from *Ggcx^{ff}; Ins1-Cre* and *Ins1-Cre* mice at 11 mM glucose. Data are represented as the AUC of the Fluo-4 and Fura Red ratio before and after verapamil addition (n = 4).

(H) Fasting serum insulin level measured in *Ggcx^{ff}; Ins1-Cre* and *Ins1-Cre* mice fed an HFD before and after verapamil treatment (n = 5–19).

(I) Proposed model for the role of γ-carboxylation in β cells (created with BioRender).

Results represent the mean ± SEM. Unpaired, 2-tailed Student's t test was used in (B), (C), (E), and (F). Two-way ANOVA with Bonferroni's post tests was used in (G) and (H). ***p < 0.001, **p < 0.01, *p < 0.05. See also Figure S7.

KEY RESOURCES TABLE

REAGENT or RESOURCE	SOURCE	IDENTIFIER
Antibodies		
mouse anti-β-Actin	MilliporeSigma	Cat# A1978; RRID:AB_476692
rabbit anti-A/E-GRD	This paper	NA
rabbit anti-cleaved Caspase-3	Cell Signaling Technology	Cat# 9661; RRID:AB_2341188
rabbit anti-FLAG	Cell Signaling Technology	Cat# 14793; RRID:AB_2572291
mouse anti-FLAG	MilliporeSigma	Cat# F1804; RRID:AB_262044
rabbit anti-GAPDH	Cell Signaling Technology	Cat# 5174; RRID:AB_10622025
rabbit anti-GFP	ProteinTech	Cat# 50430–2-AP; RRID:AB_11042881
rabbit anti-GGCX	ProteinTech	Cat# 16209–1-AP; RRID:AB_2110874
rabbit anti-Gla	Lacombe et al.[26]	NA
rabbit anti-GRP78/BIP	ProteinTech	Cat# 11587–1-AP; RRID:AB_2119855
rabbit anti-HA	Cell Signaling Technology	Cat# 3724; RRID:AB_1549585
rabbit anti-insulin	Santa Cruz Biotechnology	Cat # sc-9168; RRID:AB_2126540
goat anti-insulin	Santa Cruz Biotechnology	Cat# sc-7839; RRID:AB_2296108
mouse anti-Myc	Cell Signaling Technology	Cat# 2276; RRID:AB_331783
rabbit anti-phospho(S724)-IRE1	Abcam	Cat# ab124945; RRID:AB_11001365
rabbit anti-phospho(Ser139)-Histone H2A.X	Cell Signaling Technology	Cat# 9718; RRID:AB_2118009
rabbit anti-STIM1	Cell Signaling Technology	Cat# 5668 RRID:AB_10828699
rabbit anti-VKORC1	Ferron et al.[13]	NA
Alexa-Fluor 488-conjugated donkey anti-rabbit	Jackson Immunoresearch Laboratories	Cat# 711-545-152; RRID:AB_2313584
Alexa-Fluor 594- conjugated donkey anti-goat	Jackson Immunoresearch Laboratories	Cat# 705-585-147; RRID:AB_2340433
Biological samples		
Human cadaveric islets	IsletCore at the Alberta Diabetes Institute	http://www.bcell.org/adi-isletcore.html; RRID: SCR_014387
Human cadaveric islets	Integrated Islet Distribution Program	iidp.coh.org
Chemicals, peptides, and recombinant proteins		
$^{45}CaCl_2$	Perkin Elmer	NEZ013001MC
Diazoxide	MilliporeSigma	D9035
DNaseI	Invitrogen	18068015
Fluo-4 AM	Invitrogen	F14201
Fura Red AM	Invitrogen	F3021
Liberase TL	Roche Applied Science	5401020001
M-MLV reverse transcriptase	Invitrogen	28025013
NEBuilder HiFi DNA Assembly Master Mix	New England Biolabs	E2621
PowerUp SYBR Green Master Mix	Applied Biosystems	A25741
Q5 High-Fidelity DNA polymerase	New England Biolabs	M0491
Recombinant *Streptococcus pyogenes* Cas9 protein	Synthego	SpCas9
Thapsigargin	Tocris	1138/1

REAGENT or RESOURCE	SOURCE	IDENTIFIER
Verapamil Hydrochloride	MilliporeSigma	V4629
Vitamin K_1	MilliporeSigma	V3501
Warfarin	Santa Cruz Biotechnology	SC-204941
Critical commercial assays		
Click-iT Plus TUNEL Assay kit	Invitrogen	C10617
Mouse Insulin ELISA	Mercodia	10-1247-01
NovaRED Substrate Kit	Vector Laboratories	SK-4800
Vectastain Elite ABC-peroxidase kit	Vector Laboratories	PK-6101
Deposited data		
RNA sequencing (*Ggcx^{ff}; Pdx1-Cre* islets)	This paper	GEO: GSE199319
Identification of vitamin K-dependent proteins in mouse liver by LC-MS/MS	This paper	ProteomeXchange: PXD032920 and 10.6019/PXD032920
Identification of gamma-carboxyglutamic acid residues in mouse ERGP by LC-MS/MS	This paper	ProteomeXchange: PXD032955 and 10.6019/PXD032955
Experimental models: Cell lines		
HEK 293	ATCC	CRL-1573; RRID:CVCL_0045
ASPH$^{-/-}$ HEK 293	This paper	NA
Rat insulinoma cell line INS-1 832/3	MilliporeSigma	SCC208; RRID:CVCL_ZL55
Experimental models: Organisms/strains		
Mouse: C57BL/6J	The Jackson Laboratory	RRID:IMSR_JAX:000664
Mouse: *Ins1-Cre*: B6(Cg)-*Ins1$^{tm1.1(cre)Thor}$*/J	The Jackson Laboratory	RRID:IMSR JAX:026801
Mouse: *Pdx1-Cre*: B6.FVB-*Tg(Pdx1-cre)^{6Tuv}*/Nci	National Cancer Institute	RRID:IMSR_NCIMR:01XL5
Mouse: B6.Cg-*Gt(ROSA)26Sor$^{tm14(CAG-tdTomato)Hze}$*/J	The Jackson Laboratory	RRID:IMSR JAX:007914
Mouse: *APOE-Vkorc1l1*: B6.129-*Tg(ApoE-Vkorc1l1)^{73Maf}*	Lacombe et al.[26]	NA
Mouse: *Ggcx^{ff}*: B6.129-*Ggcx$^{tm1.1Kry}$*	Ferron et al.[13]	NA
Mouse: *Vkorc1$^{-/-}$*: B6.129-*Vkorc1$^{tm1.2Kry}$*	Ferron et al.[13]	NA
Mouse: *Vkorc1^{ff}*: B6.129-*Vkorc1$^{tm1.1Kry}$*	Ferron et al.[13]	NA
Mouse: *Vkorc1l1^{ff}*: B6.129-*Vkorc1l1$^{tm1.1Kry}$*	Ferron et al.[13]	NA
Rat: Wistar IGS (outbred) rats	Charles River Canada	Strain code: 003
Oligonucleotides		
Primers for gene expression, cloning and genotyping, see Table S7	This paper	NA
sgRNA sequence: *ASPH* knockout: GGACATCTGTAGCTGTCGTT	Thermo Fisher	CRISPR671774_SGM
Recombinant DNA		
pCMV14-ASPH-XFLAG	This paper	NA
pCMV14-ASPHΔ119-308-3XFLAG	This paper	NA
pCMV14-ASPHΔ1-49-3XFLAG	This paper	NA
pCMV14-ASPHΔ95-118-3XFLAG	This paper	NA
pCMV14-ERGP-3XFLAG	This paper	NA
pCMV14-ERGPΔ119-166-3XFLAG	This paper	NA
pCMV14-ERGPΔ167-200-3XFLAG	This paper	NA

REAGENT or RESOURCE	SOURCE	IDENTIFIER
pCMV14-ERGPΔ201-254-3XFLAG	This paper	NA
pCMV14-ERGPΔ255-310-3XFLAG	This paper	NA
pCMV14-ERGP-E119–166D-3XFLAG	This paper	NA
pCMV14-ERGP-E119–310D-3XFLAG	This paper	NA
pCMV14-ERGP-E255–310D-3XFLAG	This paper	NA
pCMV14-ERGP-N+C term-3XFLAG	This paper	NA
pENTR223.1-ASPH	Transomic Technologies	Clone ID: BC166658
pET14b-6XHIS-ERGP-85–310	This paper	NA
pGEX-GST-GRD	This paper	NA
pcDNA3-D4ER	Greotti et al.[50]	NA
pcDNA3.1-GGCX	This paper	NA
pcDNA3.1-Orai1 HA	This paper	NA
pcDNA3.1-Orai1-YFP	This paper	NA
pcDNA3.1-STIM1-CFP	This paper	NA
pcDNA3.1-STIM1-Myc	Oh-Hora et al.[77]	RRID:Addgene_17732
pcDNA3.1-VKORC1	This paper	NA
Software and algorithms		
Affinity Designer v1.10.6	Serif	https://affinity.serif.com/fr/designer/
BioRender	BioRender.com	https://www.biorender.com/
Fiji	Schindelin et al.[78]	https://imagej.net/software/fiji/
GraphPad Prism software v9.3.1	Graphpad	https://www.graphpad.com
Image Lab software v5.0	Bio-Rad Laboratories	https://www.bio-rad.com/en-ca/product/image-lab-software
Inference of CRISPR Edits (ICE) Analysis tool	Synthego	https://ice.synthego.com/
jvenn	Barbou et al.[83]	http://jvenn.toulouse.inra.fr/app/index.html
Mascot 2.6	Matrix Science	https://www.matrixscience.com/mascot_support_v2_6.html
OsteoMeasure Analysis System	Osteometrics	https://www.osteometrics.com/
Proteome Discoverer	Thermo Fisher	https://www.thermofisher.com/ca/en/home/industrial/mass-spectrometry/liquid-chromatography-mass-spectrometry-lc-ms/lc-ms-software/multi-omics-data-analysis/proteome-discoverer-software.html
Scaffold v4.8	Proteome Software	https://www.proteomesoftware.com/
Statistical significance of the overlap between two groups of genes	NA	http://nemates.org/MA/progs/overlap_stats.html
StringDB v11.5	Szklarczyk et al.[82]	https://string-db.org/
Volocity v6.0	Perkin Elmer	https://resources.perkinelmer.com/lab-solutions/resources/docs/bro_volocitybrochure_perkinelmer.pdf
Zen Blue Software	Zeiss	https://www.zeiss.com/microscopy/en/products/software/zeiss-zen.html
Other		
anti-FLAG agarose beads	MilliporeSigma	A2220
Histopaque-1077	MilliporeSigma	10771

REAGENT or RESOURCE	SOURCE	IDENTIFIER
Lipofectamine 2000 Transfection Reagent	Invitrogen	11668019
Lipofectamine CRISPRMAX Cas9 Transfection Reagent	Invitrogen	CMAX00001
Teklad purified control diet (10% kcal from fat)	Envigo	TD.08806
Teklad adjusted calories diet (60% kcal from fat)	Envigo	TD.06414
Teklad global 18% protein rodent diet	Envigo	2918